ISSN 1028-8546

Volume XXII, Number 3
Section: En
November, 2016

Azerbaijan Journal of Physics

Fizika

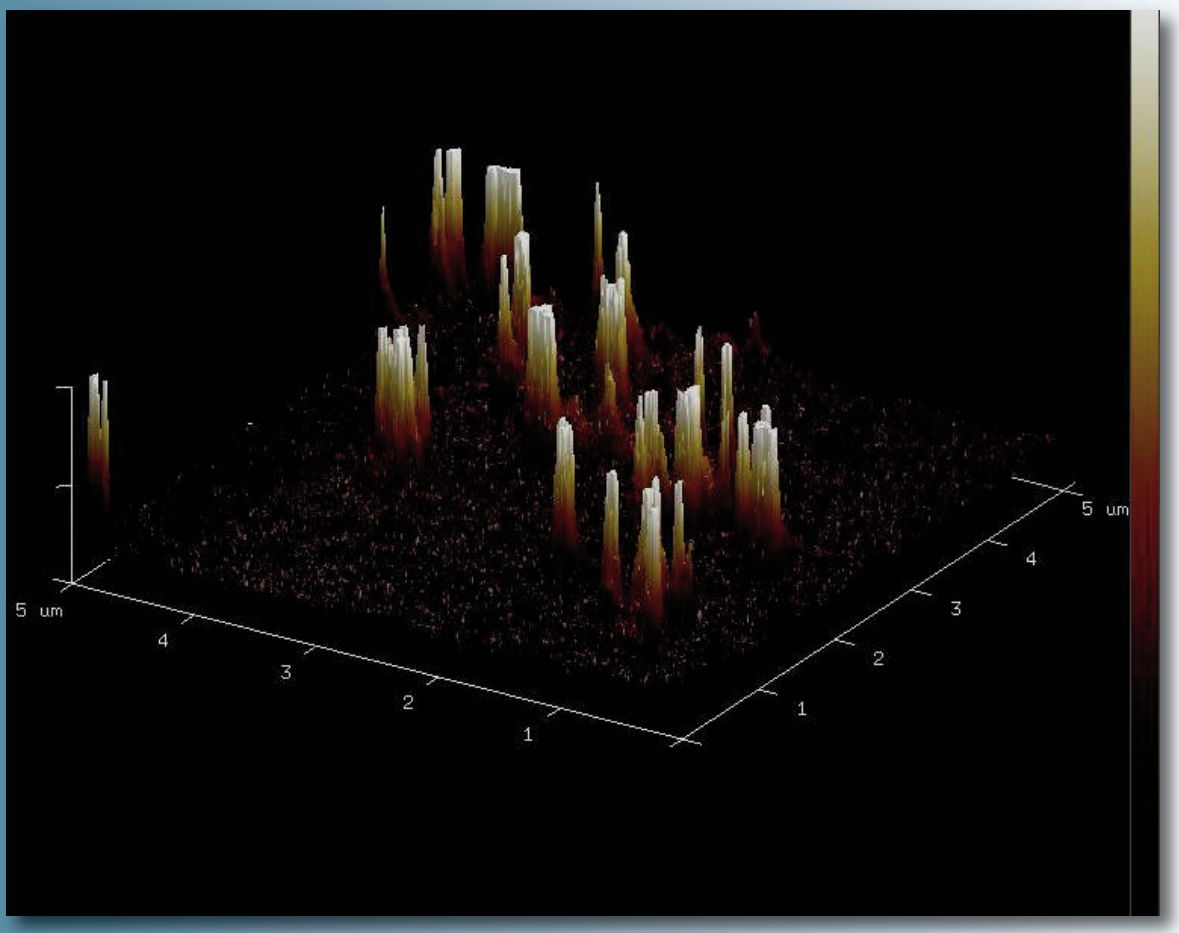

www.physics.gov.az

G.M. Abdullayev Institute of Physics
Azerbaijan National Academy of Sciences
Department of Physical, Mathematical and Technical Sciences

Published from 1995
Ministry of Press and Information
of Azerbaijan Republic,
Registration number 402, 16.04.1997

ISSN 1028-8546
vol. XXII, Number 03, 2016
Series: En

Azerbaijan Journal of Physics

FIZIKA

G.M.Abdullayev Institute of Physics
Azerbaijan National Academy of Sciences
Department of Physical, Mathematical and Technical Sciences

PUBLISHING OFFICE

131 H.Javid ave, AZ-1143, Baku
ANAS, G.M.Abdullayev Institute of Physics

Tel.: (99412) 539-51-63, 539-32-23
Fax: (99412) 447-04-56
E-mail: jophphysics@gmail.com
Internet: www.physics.gov.az

It is authorized for printing:

Published at "**SƏRQ-QƏRB**"
17 Ashug Alessger str., Baku
Typographer : Aziz Gulaliyev

Sent for printing on: __.__. 201_
Printing approved on: __.__. 201_
Physical binding:_____
Number of copies:_____200
Order:_____

LCD BACKLIGHT OPTICS

K. KÄLÄNTÄR
Global Optical Solutions, Tokyo, Japan

Optics of edge-lit backlight units (BLUs) for liquid-crystal display (LCD) are discussed in this paper. To control the direction of light in a BLU, micro-structures that their functions are based on the total internal reflection and the refraction of light are introduced. The light controlling features such as optical micro-reflectors, micro-deflectors, micro-polarizers are used on the surfaces of the light-guide plate (LGP) to shape and squeeze the light cone on the BLU. By applying the micro-features the emergent light can be directed effectively toward the LCD. These BLUs are used in video cameras, cellular phones, car navigation modules, netbooks, notebooks, monitors, TV sets, and in small size auto-stereoscopic 3D displays as well as light scanning LC devices.

Keywords: Liquid-crystal panel, LCD, backlight unit, BLU, light-guide plate, LGP, optical micro-reflector, optical micro-deflector, optical micro-prism.
PACS: 42.15.-i, 42.79.Kr, 78.66.-w.

1. INTRODUCTION

Liquid-crystal displays (LCDs) play a leading role out of various flat-panel electronic display devices, because of their excellent features such as a low power-consumption, low operating-voltage, higher resolution, full color display capabilities, large area and lightweight.

LCD is an electro-optical effect based spatial light modulator. In order to recognize the image on the LCD display a backlighting apparatus, *i.e.*, backlight unit (BLU) is required. The light generated in BLU is transmitted through the LCD and is spatially modulated by each pixel in the panel which is recognized as an image. Since LCDs have light weight, thin structure and low power consumption, LCDs are widely applied as display devices for products as cell phone, netbook, video camera, digital still camera, car navigation system, personal computer, desktop monitor, and TV set.

Mainly two structures are being used in BLUs for illuminating the LCD panels. The first one is the edge-lit (edge light) or side-light type that uses a light-guide plate (LGP) and the second one is direct view type that uses a light chamber. Light-guide plate is an important component in light controlling in an edge-lit BLU and in the same manner a light chamber is important component in direct view type BLU [1].

By using an LGP in an edge-lit BLU one can obtain a thin BLU with high luminance uniformity than the direct-view BLU. In early period of LCD panel the direct view BLUs were used. However, the demand for thinner structures boosted the usage of LGP, *i.e.*, the edge-lit type. Currently the main stream of the BLU for LCDs is the edge-lit type, and direct view type is used in large sizes.

2. LCD STRUCTURE

The basic structure of an edge-lit type backlight is shown in fig.1 (a). In this type of BLU the light control medium, *i.e.*, the LGP is an optical transparent resin, *e.g.* Polymethyl Metacrylate (PMMA), Poly Carbonate (PC), or Cyclic Olefin Polymer (COP). The LGPs are formed into a slab shape or single wedge shape. For inserting the light into the LGP, light-emitting diodes (LEDs) or cold cathode fluorescent lamps (CCFLs) are used as light sources near to one to four sides of the LGP [1].

3. LIGHT DIFFUSING FEATURE; DIFFUSING DOTS

The silk screen method has been used to print light diffusing dots on the back surface of the LGP in the conventional light guide patterning as shown in fig.1 (b). From hereafter the surface of the LGP without any feature is defined as "mirror" (M) surface and the ink-printed surface are defined as "ink" (I), so that to name the LGP as "MI-LGP" as shown in the figure. [1, 2]

In general the ink used in the pigment of printing of the LGP is Titanium Dioxide (TiO_2) that possesses high optical refractive index. The pigment includes drying solvent as main medium. Another option is to use curable ultraviolet medium with the pigment. To achieve high optical reflection in the LGP spherical beads with irregular size are used in the pigment.

Luminance uniformity on the LGP is designed by changing the size of the printed dots, *i.e.*, having a gradation of dot diameter in which the dot diameter increases at distances far from the light sources. The shape of printed dot can be a circle, square, rectangle, or diamond. These dots are positioned at the corners of hexagon shape to achieve the maximum fill factor. For example, in a 6-inch/15.24 cm diameter LGP with 3 mm thickness, the printed dispersing dot on the back surface of the LGP is a circle with a size of 200 μm near to the light sources, and 600 μm at a position far from the light sources. When the size of light dispersing dot is large, the dot is recognized from the front surface of the LCD, depending on the thickness of the LGP. Recognition of the dispersive dots can be seen in the early (1960-1980) types of the liquid-crystal displays.

In a silkscreened LGP the propagating light inside the LGP repeats the internal reflection on the inner surfaces of the LGP and the light is dispersed when hits the dots. This leads to light dispersion and color non-uniformity in the BLU. When a light source with three primary colors or a pseudo-white color is used, white light is extracted on the LGP near the light sources and reddish light at positions far from the light source. The short wavelengths such as blue and green are scattered by the printed dots. These colors are gradually removed from the propagating light. This phenomenon is the so-called sunset light dispersion that exists in the light diffusing LGPs.

131 H.Javid ave, AZ-1143, Baku
ANAS, G.M.Abdullayev Institute of Physics
E-mail: jophphysics@gmail.com

4. LIGHT DIFFUSING FEATURE; MICRO-DIFFUSER

To avoid the time-consuming printing process more efforts have been put in chemical etching of the injection metal mold tool in which an optical flat surface of a mold that is used as back surface of an LGP in injection, is designed to have a pattern with etched (E) feature. The metal mold is used in a cavity on injection machine. The hot resin is shaped in the injection cavity and the pattern is transferred on to the resin to make an LGP with etching features [1, 2]. As shown in fig.1(c), the etching features are transferred onto the back surface of the LGP, and the front surface of the LGP is flat, *i.e.*, "mirror-like", so that the LGP is defined as "ME-LGP". To extract part of the propagating light from the LGP a uniform replication pattern of the etching features fabricated on an etched metal mold and is transferred onto the front surface of LGP in an injection mold. If the both the front and back surfaces of an LGP are replications of the etched features, the LGP is defined as "EE-LGP", *i.e.*, "Etching-Etching" LGP.

The size of an etching feature is about 200 μm. For making uniform luminance on the BLU, a density gradation of etching feature is applied to LGP in which the distance between the features decreases as the distance from the light sources increases. This is shown in fig.1 (d). In case of "EE-LGP", the front surface pattern is a uniform, *i.e.*, the distance between the etched dots is constant. However, to avoid interference between the LGP pattern and the prism films that are used on the LGP, the dot position is randomized frequently. By using the precisely etched molds and replication process, (injection mold), the time spending for printing, can be saved. In addition, the issues regarding the pigment density differences or diffusing feature size can be avoided.

To increase the diffusing function of the LGP, micro-size diffusing beads are added to the material of the LGP. Another option is to make fine diffusing features on the front surface of the LGP. This can be realized by replication of a diffusing mold pattern onto the LGP's front surface [3].

The LGPs explained in this section are light diffusing types in which one or two surfaces (front and back surfaces) of the LGP are replication of the etching feature. In a diffusing LGP the direction of the dispersed light is not controlled, thus resulting in light loss in the BLU.

To enhance the luminance on the LGP a light direction controlled LGP that can collimate the extracted light into a narrow light cone is required.

5. LIGHT REFLECTING FEATURE; MICRO-REFLECTOR

To control the direction of the extracted light and avoid issues of chemical etching, a TIR based micro-reflector has been developed. LGPs with optical micro reflectors (MRs) are shown in fig.2 [1, 4-6]. An MR feature has a shape of micro-lens or micro-prism with optical surface. The MR features are structured on the back surface of an LGP [7-16]. Each MR feature reflects light based on the total internal reflection (TIR).

To provide a uniform extracted luminance on the BLU, an array of MR features are fabricated on a metal mold with an optical surface. The pattern of the mold is transferred onto a LGP in an injection molding. The MR feature is often a concave or convex micro-lens with round, square, elliptical or diamond geometrical shape [1, 8]. An MR feature reflects substantial portion of the rays that are incident on the inner surface of the feature. A portion of the light rays that could not satisfy the TIR condition is refracted on the inner surface of the feature. The refracted light leaks toward the back surface of the feature. A reflector film is used near to the features to reflect back the leakage light into the LGP (fig.1).

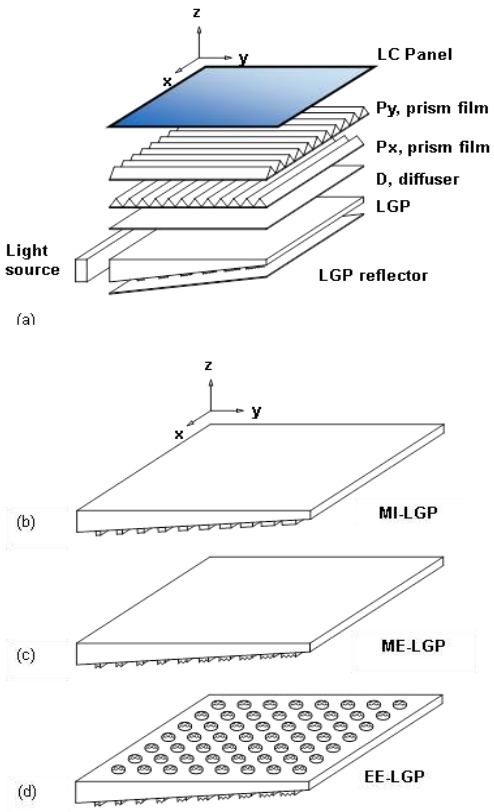

Fig.1. (a) is structure of a conventional LCD BLU. The LGPs with light diffusing features are shown in (b), (c), and (d). *(b)* is LGP with light diffusing printed (silkscreened) dots. *(c)* is LGP with replicated light diffusing dots. *(d)* is LGP with replicated light diffusing dots on the front and back surfaces.

Since the front surface of the LGP is "mirror-like" (M) and the back surface is a density gradation (G) of the MR features, the LGP is defined as "MR_G-LGP". In case of uniform pattern of MRs with constant pitch, the LGP is "MP_U-LGP". To enhance the TIR function of the MRs the tangent of the concave surface or the angle of reflection should be kept constant, *i.e.*, the surface should be as close as to a "V" shape prism surface.

To boost the collimation of the extracted light on the LGP, an array of micro-lines with "V" shape is fabricated on the back surface of the LGP. In this case the LGP is defined as "MP-LGP". The function of the MR feature is to reflect the propagating light without losing the light energy and to direct the extracted light into a light cone (solid angle). By controlling the reflection angle of the

features the emergent light cone angle is controlled resulting in an increase of luminous flux and luminance on the BLU.

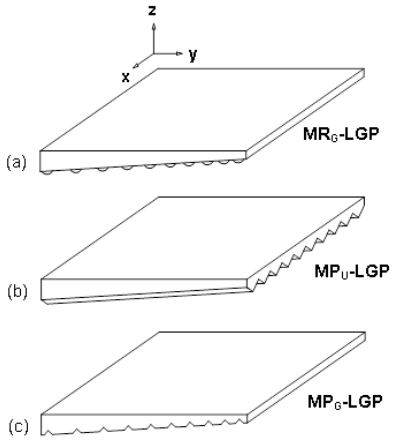

Fig. 2. LGPs with light reflecting features. *(a)* is LGP with omni directional MR_G features. *(b)* is LGP with uniform light collimating prism array along y-axis. *(c)* is LGP with graded position for linear prism along the x-axis.

The size of the MR feature is about few microns and in comparison with light diffusing dots or etching features, the MR features are small and not recognizable from top of the BLU through the LC panels.

Figure 3 shows cross-sections of the prismatic MR features that are often used to extract the light in LGPs. Depending on the shape of the prism, the zenith angles (with respect to LGP's surface normal) of extracted light rays increase. When the prisms shown in fig.3 (a), (b) are used, the emergent light have a large zenith angle on the LGP. The BLU structure and the light deflection concept are shown in fig.4 (a) and (b). Therefore, a prism film with total internal reflection (TIR prism), the so-called inverted prism, is required on the LGP to direct the emergent rays toward the normal surface of the LGP [17]. The prism structure shown in fig.3(c)-(f) extracts the propagating light rays toward the normal in which the zenith angles are reduced. To provide a uniform luminance, two methods are mainly used. In the first method, the prism angle is fixed and the pitch is varied. In the second method the pitch is fixed and the prism angles are varied. The parameters given in the figure are important for fixing the shape of the prism or designing a pitch gradation of the prisms. A graded-pitch prismatic LGP can be designed to have small emergent zenith angle for the extracted light. Such a prismatic LGP can be used with a low haze diffuser film without using any light directing or collimating film. The light cone of such a LGP is narrower than the light diffusing type LGP. When the prismatic MR features are used as light extraction, the light diffusion or wavelength dispersion is absent in the LGP.

6. LIGHT DEFLECTING FEATURES; MICRO-DEFLECTOR

To provide a direction controlled light cone on the front surface of a LGP, the MR features shown in fig.3 are structured on the back surface of the LGP [1]. Figure 5 shows the LGPs with light ray micro-deflector (MD) on the front surfaces. The MD features are being fabricated on the mold tools similar to that of MR feature and are being transferred to a LGP using injection molding.

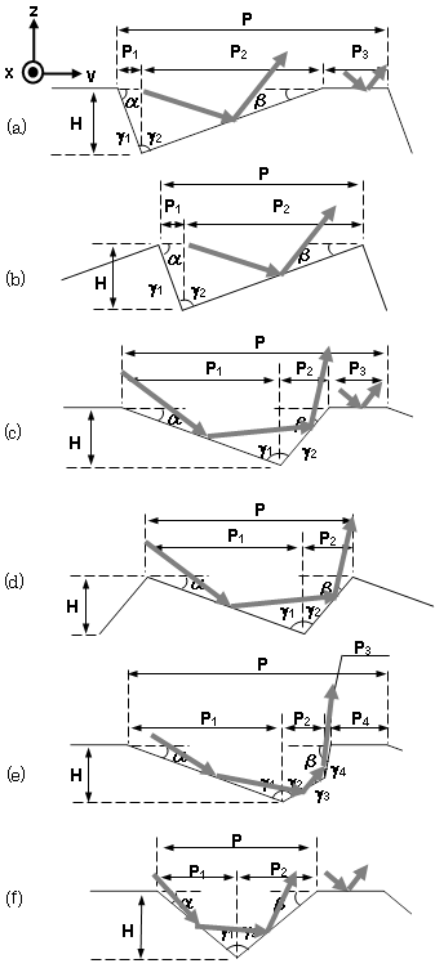

Fig.3. (a) Prism structures for light extraction. *(b)* Prisms that extract the light in a way that the zenith angle of the emerged light increase with respect to the surface normal. *(c), (d), (e), and (f).*The prisms that extract the light in a manner that the zenith angle decrease with respect to surface normal.

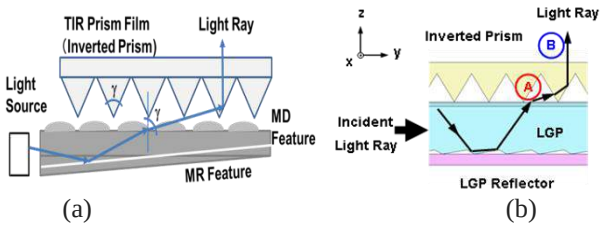

Fig.4. Principle of light ray deflecting in a BLU with functional LGP and inverted prism film. *(a)* BLU cross section, *(b)* Light deflection concept.

In a MD-LGP a light ray repeats total internal reflections before hitting a single MD feature. When a ray is incident on the inner surface of a MD feature, the ray is deflected (on refraction) and directed on the MD feature. To form the emergent light cone and to control the light

direction, the geometrical shape of the micro-deflector feature is designed and matched to the MR feature.

In the design of a LGP the required emergent light can be assumed and the arrays of micro-reflectors and micro-deflectors are designed in combination.

7. LIGHT POLARIZING FEATURES; MICRO-POLARIZER

A micro-prism shaped on the back surface of LGP separates the propagating light into reflecting and refracting light [1]. As shown in fig.6, the incident light onto the prism surface is polarized into S-polarization, perpendicular to the incident surface, and P-polarization, parallel to the incident surface. The reflection factors for these polarizations are different. However, when the reflection factor of the P-polarization approaches to zero, the incident angle is the so-called Brewster angle. Under the Brewster condition the reflected ray is perpendicular to the refracted light ray, *i.e.*, the angle between these two rays is 90° ($\theta_r + \theta_t$=90°), where the incident angle is θ_i, the reflection angle is θ_r, and the refraction (transmitted) angle is θ_t. The Brewster angle is given by $\theta_B = tan^{-1}[1/n\ (\lambda)]$, where the refractive index of the prism material is n (λ). In case of PMMA, the refractive index $n(\lambda_D)$ is equal to 1.492 at D-line (λ_D=589.3 nm) of the Sodium and the Brewster angle is about θ_B=33.8°. The Brewster polarization angle is defined for a single light ray. Therefore a portion of the propagating light rays can satisfy the polarization condition. The prism with Brewster angle can be designed by considering the propagating rays angles'.

8. LIGHT SHAPING FEATURES ON INCIDENT PLANE; ROUNDED MICRO-PRISM

In an edge-lit type BLU few LEDs or tens of LEDs are used near to the light introduction surface (one of the sides) of a LGP depending on the application, the size, the amount of luminance, or an optimized angular luminance distribution [18]. When the light introduction surface of an LGP is flat, the introduced light of the LED is being refracted on the light introduction surface and as a result the rays are being deflected toward the surface normal on the inner surface (light introduction surface). The maximum possible angle of an introduced ray is corresponding to the critical angle $\theta_C = sin^{-1}(1/n_{LGP})$, where n_{LGP} is the refractive index of the LGP. The light distribution inside the LGP is limited within the critical angles cone and a dark zone appears between two internal distributions (between two LEDs). The zone contributes in non-uniformity of the luminance distribution on the BLU. To reduce or eliminate the non-uniformity, an array of micro-structures (rounded micro-prism) are fabricated on the light introduction surface to widen the internal light distributions, or increase the refracted light cone as shown the structures in fig.7. The array of micro-structures widens the light distribution inside the LGP that results in reducing the dark zone and increasing uniformities on the LGP. The light distribution cone is limited to about +/-42° (n_{LGP} =1.492, PMMA) when the light introduction surface is flat. However, when the rounded micro-prisms are used on the light introduction surface the distribution is widened to +/-57° (fig.8). By providing the micro-structures, the inserted light increases that results in reducing the Fresnel loss and an increase in coupling efficiency by 5%. For comparison the coupling efficiency for a slab LGP is about 82%.

9. LIGHT SHAPING FEATURES ON INCIDENT PLANE; LENTICULAR LENS ARRAY

To shape and to control the direction of the light inserted into the LGP, an incoherent diffraction grating is

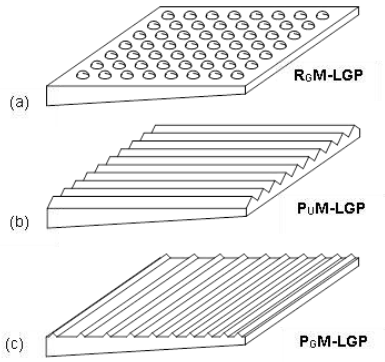

Fig. 5. LGPs with light deflecting features.*(a)*is Omnidirectional features, *(b)* is uniform unidirectional light deflecting features, *(c)* is position-graded light deflector features on the front surface of the LGPs.

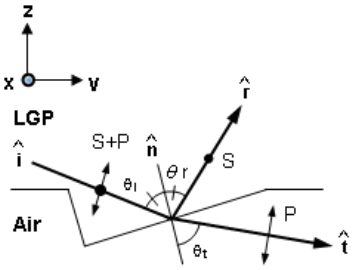

Fig.6. Light polarizing feature. The polarizing features separate the S is wave and P is wave on reflection. These are structured on the back surface of the LGP.

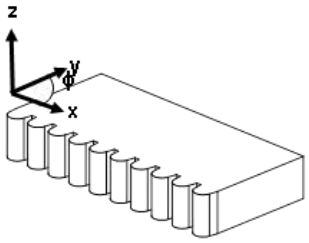

Fig.7. Micro-optical features on the light introduction surface of the light-guide plate. These structures widen the spatial light distribution of the inserted light inside the LGP.

structured on the back surface of the LGP near to the light introduction surface as shown in fig.9. As an example a grating with a pitch of P=240 μm, a width of W=120 μm, a height of H=32 μm, a radius of R=72 μm, a length of L=2 mm is designed in an LGP with a thickness of t=0.8 mm for cell phone BLU application. The thickness

or the number of the LEDs is the parameters in designing of the gratings where the size can be few microns to tens of microns. In addition, the shape can be "V" prism, rounded prism or lenticular lenses depending on the distribution of the inserted light on the inner surface of the light introduction surface. Due to the shape of the gratings the light can be directed toward sides of the LGP or toward the surface on the opposite surface (against the light source). The gratings shape the propagating light and as a result shaping the emergent light on the LGP. Therefore, the dark zone reduces and leads to decrease in the dark zones, *i.e.*, an increase in the bright area, and finally an increase in the uniformity near the light source on the LGP.

10. LIGHT SOURCES FOR BACKLIGHT; PSEUDO-WHITE LED

An LED is a solid-state lighting feature that is based on the PN junction of gallium nitride (GaN) compound semiconductor light-emitting material [1]. A pseudo-white LED is a combination of Indium mixed GaN that has a light emitting quantum well structure, and YAG phosphor layer that covers the semiconductor chip (fig.10).

A pseudo-white LED is based on phosphor excitation and wavelength conversion. The chip emits blue light that excites the surrounding phosphors layer of yellow light. The blue light is scattered and absorbed by the phosphor. Since the blue and yellow light are complementary colors, the result of color combination is a white color.

In recent years, the pseudo-white LEDs are widely used in the backlights of the handy terminals, such as cell phones, netbooks, and notebooks computers. Top-view LEDs are used in car navigation systems and side view LEDs are used in notebook PCs and netbooks. By using these small pseudo-white LEDs, thin and light weight units and modules are realized. The LEDs are being merged into the display backlight of various sizes. Therefore, the demands for LEDs with higher efficiencies and different packages are widely highlighted.

High efficiency monochromatic LED light sources of red (R), green (G) and blue (B) have been developed in recent years, and used as primary colors in LCD backlighting unit. Blue and green are the chips of compound semiconductors of InGaN, and red LED is a compound of four semiconductors, *i.e.*, AlInGaP (Aluminum, Indium, Gallium, and Potassium). These LEDs are used in a backlight and a white point is obtained based on the additive color mixing. Because of the large dependency of the LEDs on the temperature, a light sensor is installed in the BLU to stabilize the BLU, especially in large size displays. The three-primaries used BLUs have wide color production gamut that can be used in the applications of image editing and design. However the tolerances between colors of the LEDs or low electro-optical conversion efficacy and high cost of the LEDs, are the barriers in employing of the LED with primary colors to display backlights. Despite of great attempt to use primary colors in BLUs, Sony Corporation announced all LED display in Los Vegas Consumer Electronic 2012.

11. LIGHT SOURCES FOR BACKLIGHT; COLD CATHODE FLUORESCENT LAMP

A cold cathode fluorescent lamp (CCFL) was being used in large size LCD displays until the recent years. A CCFL is made of two electrodes mounted at each side of fluorescent glass tube of any shape, includes an appropriate amount of Mercury (0.5-1.0 mg) and encloses an inert gas (Argon). The fluorescent materials include three wavelengths phosphor that is coated on the inner wall surface of the tube [1]. When a high voltage is applied between the electrodes, the electrons are drawn toward the electrodes present inside the tube as shown in fig.11. The electrons collide with the mercury molecules in the tube and as a result of collision ultra violet light is emitted. The ultraviolet light excites the phosphor that leads to white light conversion.

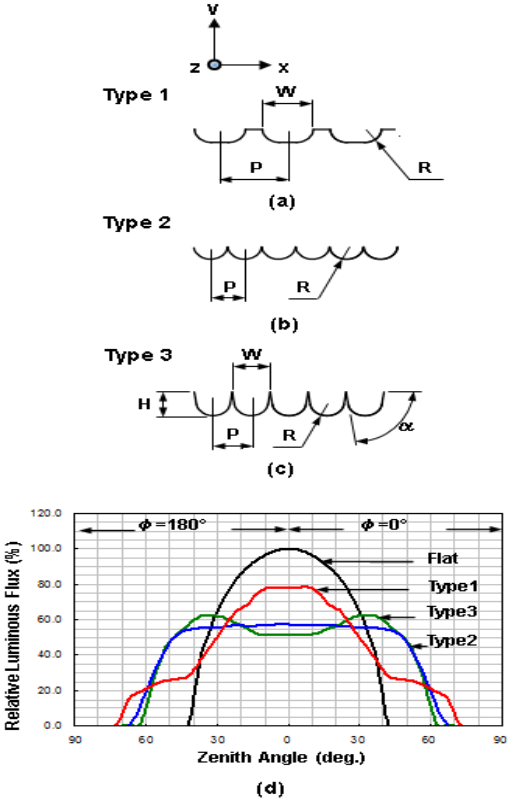

Fig.8. Structures used on the light introduction surface of a LGP for light shaping inside the LGP. *(a),(b)* and *(c)* are cross-sections of three types of features. *(d)* is light intensity distribution in a LGP using the features shown in (a), (b) and (c). Flat is the surface without micro-structure that is shown for comparison.

The CCFLs of 3 mm in diameter were used in the large TV sets or monitors. However, the recent movements on prohibition of the mercury which is a toxic material, and the recent development of high efficacy pseudo-white LEDs boost the usage of the LEDs in the display BLUs.

12. CONCLUSIONS

A backlight functions as illuminant unit at the rear of liquid crystal panel and plays an important role in reducing power consumption and improving the display

characteristics. The advances in light emitting devices, their driving methods and the function of a light-guide plate that configures a backlight are explained in this paper.

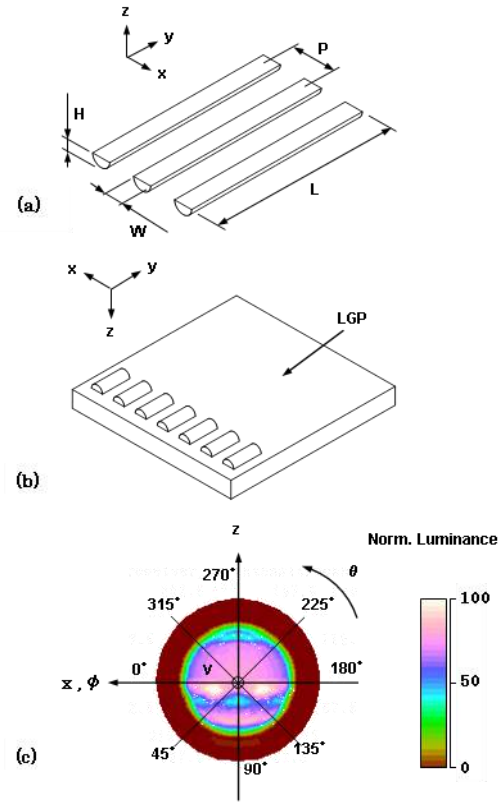

Fig.9. Structures used on the light introduction surface of a LGP for light shaping inside the LGP. (a),(b) and (c) are cross-sections of three types of features. (d) is light intensity distribution in a LGP using the features shown in (a), (b) and (c). Flat is the surface without micro-structure that is shown for comparison.

A light-guide plate is used not only to make a uniform luminance but also for dispersing, reflecting, deflecting or shaping the emergent light. A backlight unit with a wide angular luminance distribution can be realized by using a light dispersing LGP. A backlight unit with controlled angular luminance distribution can be obtained by employing a LGP that is featured by micro-reflector features [19-22]. The angular luminance can be squeezed by combining the light deflecting and the micro-reflecting features in a LGP [20,22]. A variety of light shaping BLU can be realized by selecting proper light reflector and deflector features.

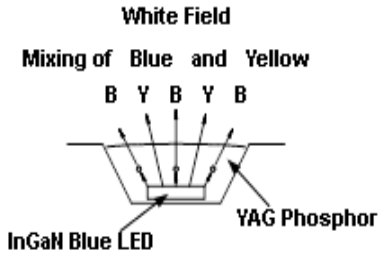

Fig.10. Pseudo-white LED. A blue light emitting chip (InGaN) is covered with the yellow fluorescent agent; YAG. The additive complementary colors mixing result in white color light.

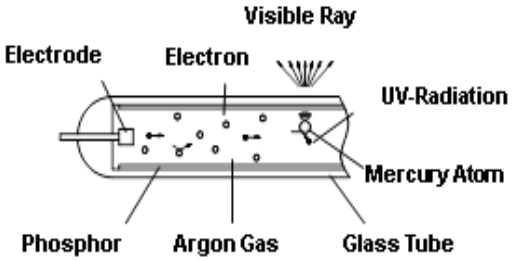

Fig.11. Structure of a CCFL. Small amount of Mercury (0.5-1.0 mg) and inert gas (Argon) are encapsulated in the tube.

In the near future, the divergence applications of versatile LCD are expected. Therefore, a thin and highly functional LGP that results in realization of low power consumption BLU is necessary.

---

[1] *K. Käläntär*. LCD Backlight Technology, (2006), CMC Publishing Co. Ltd. (in Japanese).

[2] *K. Käläntär*. Monthly Display, June issue (2003) (in Japanese).

[3] *Y. Koike*. Spring Conference of the 41st Society of Polymer Science, No. IL -27

[4] *K. Käläntär*. Digest-C5 Fine Process Technology Japan 1997 7th Seminar, pp.11-18 (1997) (in Japanese)

[5] *M. Ohe*. Flat Panel Display '93, pp.137 (1992/11).

[6] *A. Tanaka*. Proc IDW'98, pp.347-350 (1998).

[7] *K. Käläntär*. SID99 Technical Digest, pp.764-766 (1999).

[8] *K. Käläntär, et al*. IEICE Trans. Electron, Vol.E84-C, No.11, pp1637-1645 (2001).

[9] *K. Käläntär, et al*. SID00 Technical Digest, pp.1029-1030 (2000).

[10] *K. Käläntär, et al*. Proc IDW'00, FMCp-8, pp.463-466 (2000).

[11] *K. Käläntär*. Proceedings, IDW'02 FMCp-10, pp.549-552 (2002).

[12] *K. Käläntär*. Monthly Display, Vol.7, No.1, pp.68-72 (November 2001) (in Japanese).

[13] *K. Käläntär*. JSAP, AM-FPD 2008, pp.101-104 (2008).

[14] *K. Käläntär*. EKISHO Vol.12, No.1, pp.31-38 (2008).

[15] *T. Uchida*. "Display" Supervisor, Industrial Commission, pp.96-100 (2006). (in Japanese).

[16] *K. Käläntär*. "Digest of Practical Optics", ISBN 4-901677-62-4, Book Chapter 15, pp.338-360, 2006 (in Japanese).
[17] Guidelines of prism sheet for LCD backlight, technical art S/M16X Diamond Series (Mitsubishi Rayon Co., Ltd.) (in Japanese).
[18] *K. Käläntär*. SID2007 Technical Digest, 33.3L, 1240-1243, (2007).
[19] *K. Käläntär*. "Optical Characteristics of Directional BLU for Field-Alternate Full Resolution Auto-Stereoscopic 3D LCD," in *Journal of Display Technology,* , vol.12, no.1, pp.71-76, Jan. 2016.
[20] *K. Käläntär*. *"*A Directional Backlight with Narrow Angular Luminance Distribution for Widening Viewing Angle of a LCD with a Front-Surface-Light-Scattering Film" J. Soc. Inf. Display April (2012).
[21] *K. Käläntär et al.* "A monolithic segmented functional light guide for 2-D dimming LCD backlight" J. Soc. Inf. Display 19 37 (2011).
[22] *K. Käläntär et al.*"Backlight unit with double-surface light emission using a single micro-structured light-guide plate ", J. Soc. Inf. Display 12 379 (2004).

Received: 26.05.2016

INVESTIGATION OF DISADVANTAGES OF LFS SCINTILLATOR

F.I. AHMADOV [1,3], Z.Y. SADYGOV [1,2], E.A. JAFAROVA[4], R.S. MADATOV[3], A.A. DOVLATOV[4], G.S. AHMADOV [1,2], A.Z. SADIGOV [1,3], S.S. SULEYMANOV [1,3], R.A. AKBEROV[1,3], N.N. HEYDAROV[1], M.S. NAZAROV[1]

[1] *National Nuclear Research Centre of MCHT, Baku, Azerbaijan.*
[2] *Joint Institute for Nuclear Research, Dubna, Russia.*
[3] *Institute of Radiation Problems of ANAS, Baku, Azerbaijan.*
[4] *Institute of Physics of ANAS, Baku, Azerbaijan.*
e-mail: farid-akhmedov@yandex.ru

In this paper two main disadvantages of LFS scintillator. There are intrinsic background, which limited their using for low background applications, and trapped time of metastable state that makes worse energy resolution of detector.

Keywords: avalanche photodiode, scintillator, gamma ray, HPGe, detector.
PACS: 07.77-n; 07.77.-Ka; 29.40Wk; 85.30De; 85.60Dw

INTRODUCTION

Last years scintillators with high light output are widely used in different areas of science and industry [1-7]. Basic requirements to the scintillation materials are fast response, high light output, high density, and high atomic number (Z) [1]. Lutetium Fine Silicate (LFS) has extremely high density of 7.4 g /cm^3, as well as a high Z value (Z=64), making this crystal very attractive for manufacturing highly efficient detectors. Scintillation detector based on LFS scintillator was widely investigated and it was obtained that this scintillator was optimal one for PET scanners and electromagnetic calorimeter [3, 4]. At the same time, LFS scintillator has several disadvantages: LFS has a naturally occurring isotope $_{176}$Lu which emitted beta particle and gamma rays, LFS scintillator has trapping center (metastable state), where trapped electron stayed for a long time and these centers are main reason in delayed light emission [1]. These disadvantages decrease its usefulness for low background applications and decreases amplitude of detected gamma ray due to metastable state [7].

That is why this work is dedicated to investigate two main disadvantages of LFS scintillator: intrinsic background and trapped time of metastable states.

II. EXPERIMENT DETAILS AND RESULTS

Two different sized LFS (Lutetium Fine Silicate) scintillators is used (3×3×0.5 mm^3, 3×3×10 mm^3) in this work. Its decay time was 19 ns. The LFS-8 gives the light yield of 30000 photons/MeV deposited energy. The maximum wavelength of light emission is 422 nm. The sides of the LFS-8 crystals were wrapped into three layers of 0.1 mm thick white Teflon tape except one face open to join with the MAPD with silicone grease. The MAPD-1P was operated in Geiger mode. The used MAPD consisted of a silicon substrate of n-type conductivity (wafers with a specific resistivity in the range from 10 to 30 Ω×cm) on which two silicon epitaxial layers of p-type conductivity were grown (7 Ω×cm). The device also contains a matrix of independent n+-type pixels buried deep in the epitaxial layers mentioned above. The design and operation of the device were described in [6-8]. The used MAPD device had a 3×3 mm^2 active area and total pixel number was 1.35×10^5. The maximum photon detection efficiency of the MAPD was about 30% around 450-525 nm light wavelengths. In the gamma ray measurements, the MAPD signal was sent to preamplifiers (gain=30).

The signal from the preamplifiers was sent to CAEN DT5720 digitizer module with 12-bit resolution and 250 MS/s sampling rate. All measurements were carried out at room temperature and without shielding materials (or box).

The pulse-height spectra of the $_{113}$Sn source with different sizes of LFS scintillator is shown in fig.1. $_{113}$Sn activity was 70 Bq and measurement time was 1,800 seconds in the experiment. External and intrinsic background of LFS (due to $_{176}$Lu) strongly affected on the low energy tail of spectrum of $_{113}$Sn source due to low source activity. Photo peak of $_{113}$Sn is invisible at spectrum due to intrinsic radiation of LFS. Intrinsic radiation of LFS is reduced by decreasing thickness of LFS scintillator (3×3×0.5 mm^3) and in this way photo peak of $_{113}$Sn is separated perfectly from background. Energy resolution of 391.7keV gamma ray from $_{113}$Sn was 20%. The intrinsic radiation of LFS (3×3×10 mm^3) is investigated by high purity germanium (HpGe) detector. The measurement time was 2x10^4 seconds. Obtained activity and mass of Lu-176 were 23.5±3 Bq and 12.5 mg respectively. Four major gamma lines were observed in the spectrum: γ-54.4 keV (25.9%), γ-88.3 keV (13%), γ-201.6 keV (84%), γ-306.3 keV (93%) and a sum of the last two γ-507.9 keV (0.8%) [1].

Second main disadvantage of LFS-8 scintillators is sensitivity to light. When the scintillator LFS-8 stays under light for a long time the photon generates an excited electron which are captured by activator and trapping centers (also metastable states).

The trapped electrons in metastable states transited to the ground state by emitting delayed scintillation photons which will play a key role in background current.

131 H.Javid ave, AZ-1143, Baku
ANAS, G.M.Abdullayev Institute of Physics
E-mail: jophphysics@gmail.com

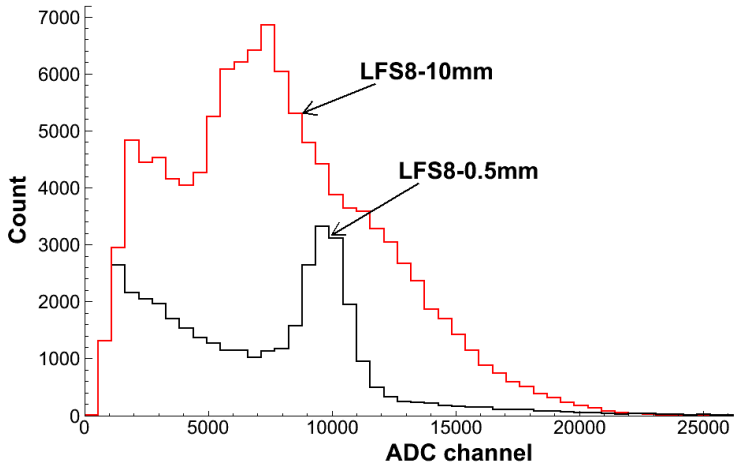

Fig. 1. The pulse-height spectra of the $_{113}$Sn source with different sizes of LFS scintillator.

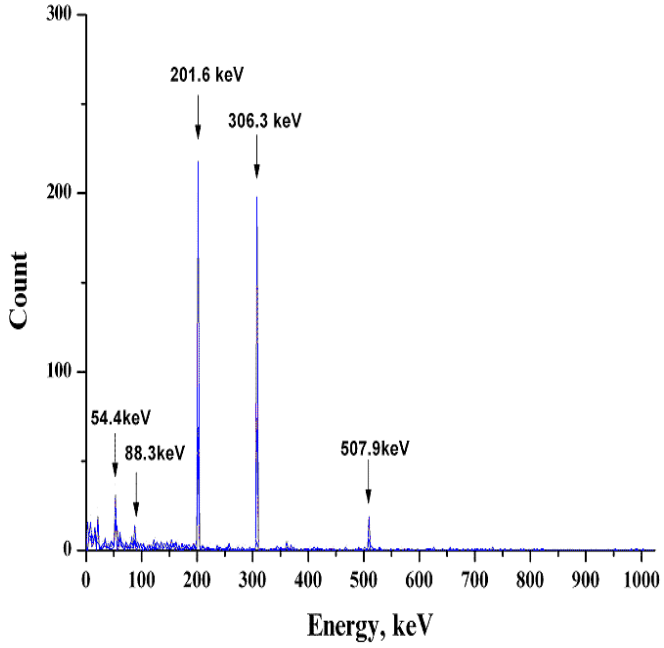

Fig. 2. Energy spectrum of gamma rays from the natural radioactivity in the LFS (Lu-176) measured using HPGe detector.

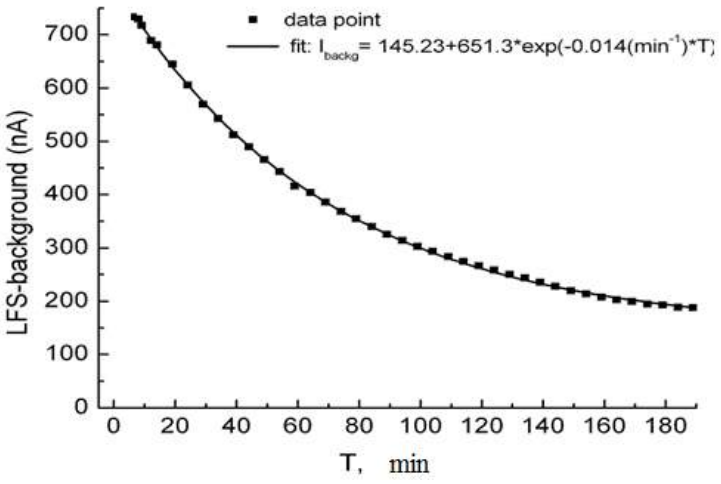

Fig 3. The internal excited background of LFS scintillator dependence of time.

In fig 3 showed dependence of change of background current of MAPD diode on time for the LFS-8 scintillator which stayed under light for long time. The scintillation photons which emitted from LFS scintillator detected by MAPD-3A photodiode. The sides of the LFS-8 crystals were wrapped into three layers with thickness of 0.1 mm of white of teflon tape except one face open to join with the MAPD with silicone grease and kept in the dark box for one day. The internal dark current of diode was 180nA at the operating voltage and all experiments was carried out at room temperature. LFS scintillator was irradiated with light (for 20 minute) and after that, background current was increased sharply to 730nA. The background decreased exponentially law with time**:** $I_{backg}(nA)=145.23+651.3\times\exp(-0.014(\min^{-1})\times T)$ here T-time and I_{backg} –background current. It was defined that background current reached to previous internal dark current of diodes during 170 minute. For this reason LFS-8 scintillator have to be protected during measurements from external light source. During gamma ray detection, some of scintillation light delayed for long time due to the trapped electron by metastable state. The amplitude of gamma ray is reduced by amount of excited electron which trapped by metastable state and this makes worse energy resolution of detector.

CONCLUSION

Two disadvantages of LFS scintillator was investigated in this work. Intrinsic background of larger size LFS (due to $_{176}$Lu) is measured with HPGe detector. Obtained activity and mass of $_{176}$Lu were 23.5±3 Bq and 12.5 mg respectively. Intrinsic radiation of LFS was reduced by decreasing thickness of LFS scintillator ($3\times3\times0.5$ mm^3) in this way photo peak of $_{113}$Sn (low activity) is separated perfectly from background . Energy resolution of 391.7keV gamma ray from $_{113}$Sn was 20%.

It was obtained that the excited background current due to metastable center is decreased exponential law with time. The background current reached to initial value during 170 minute. This effect reduced the amplitude of gamma ray (due to electron which trapped by metastable state) and it makes worse energy resolution of detector.

Acknowledgments

This work was supported by the Science Development Foundation under the President of the Republic of Azerbaijan Grant No.EIF-2014-9(24)-KETPL-14/03/1.

[1] *G.F. Knoll*. Radiation detection and measurements, John Willey and Sons, Inc., New York 2000.

[2] *Z. Sadygov, F. Ahmadov, X. Abdullaev et al*. Development of scintillation detectors based on micro-pixels avalanche photodiodes, *Proceedings of Science*, 2012, (PhotoDet 2012) 37.

[3] *Yu. D. Zavartsev, M. V. Zavertyaev, A. I. Zagumenny i, A. F. Zerrouk et al*. New radiation resistant scintillator LFS-3 for electromagnetic calorimeters, Bulletin of the Lebedev Physics Institute, 2013, vol. 40, Issue 2, p. 34-38.

[4] *A. Nassalski, M. Moszyński, A. Syntfeld-Każuch et al.* Multi Pixel Photon Counters (MPPC) as an Alternative to APD in PET Applications, *IEEE Trans. Nucl. Sci.*, vol. 57, iss.3, p.1008 -1014 2010.

[5] *Z. Sadygov, A. Olshevski, I. Chirikov et al*. Three advanced designs of micro-pixel avalanche photodiodes: their present status, maximum possibilities and limitations, Nucl. Instrum.Methods Phys. Res., Sect. A 567, 70–73 (2006).

[6] *Z. Sadygov, F. Ahmadov et al*. Technology of Manufacturing Micropixel Avalanche Photodiodes and a Compact Matrix on Their Basis, Physics of Particles and Nuclei Letters, 2013, vol. 10, No. 7, p. 780–782.

[7] *F. Ahmadov, G. Ahmadov, E. Guliyev, S. Khorev, R. Madatov, R. Muxtarov, J. Naghiyev, A. Sadigov, Z. Sadygov, S. Suleymanov, F. Zerrouk.* Development of compact radiation detectors based on MAPD photodiodes with Lutetium Fine Silicate and Stilbene scintillators, Journal of Instrumentation, 2015, vol. 10, p. 1-7.

[8] *Z.Ya. Sadygov*. Russian Patent № 2316848, priority from 01.06.2006.

Received: 27.04.2016

CATHODOLUMINESCENCE CHARACTERISTICS OF $SrAl_2O_4$: Eu^{2+} NANOPHOSPHORS AT LOW TEMPERATURES

S.A. MAMMADOVA[1], R.B. JABBAROV[1,2]
G.M. Abdullayev Institute of Physics, Azerbaijan NAS, Baku, Azerbaijan[1]
Research and Devolopment Center for High Technologies, Ministry of Communications and Information Technologies[2]

This paper reports CL characteristics of nanosized $SrAl_2O_4$:Eu^{2+} phosphor. This sample was prepared by combustion method. X-ray diffraction (XRD), cathode luminescence (CL) were conducted to characterize the phosphor. The comparison between the emission spectra revealed that pure and Eu doped $SrAl_2O_4$ samples showed the same peaks at 375 nm. This peak is attributed to crystal defects.

Keywords: nanophosphor, combustion method.
PACS: 33.50.-j, 33.50. D

INTRODUCTION

Due to their excellent luminescence properties, high quantum efficiency in visible region, good stability, color purity, excellent physical and chemical properties and the easy preparation, green $SrAl_2O_4$:Eu^{2+} alkaline earth aluminates have the potential applications in fluorescent lamps, plasma display panels, pc LEDs and persistent luminescent materials [1-5].

In this paper, Eu^{2+} doped $SrAl_2O_4$ nanophosphor was synthesized by combustion method and their cathodoluminescence properties were studied. The results of the cathodoluminescence measurements of $SrAl_2O_4$:Eu^{2+} nanophosphors were compared and discussed. The emission of these materials is highly efficient, and their emission wavelength heavily depends on host lattice. In the $SrAl_2O_4$ host lattice, the main emission band of Eu^{2+} ions is centered near 520 nm, when another emission band at 444 nm is still the object of discuss. In this article, we have observed new peak at 375 nm and our experimental results proved that this peak is related to crystal defects which help to increase a number of traps and prolong afterglow duration. We have observed 2 minutes afterglow duration in $SrAl_2O_4$:Eu^{2+} phosphor [11]. If there is not any co activator ion, then the observed long afterglow duration showed that crystal defects played the role of traps.

2. EXPERIMENTAL SECTION

All reagents were commercially purchased and used without further purification. For the synthesis, stoichiometric amounts of $Sr(NO_3)_2$ (99,99%), $Al(NO_3)_3 \cdot 9H_2O$ (99,99%), $Eu(NO_3)_3 \cdot 6H_2O$ (99,99%), $CO(NH_2)_2$ (99,3%) and H_3BO_3 (99,9%) were dissolved together in 20ml of deionized water to obtain a transparent solution. Small amount of boric acid was used as flux and urea as fuel [6,7]. The components were mixed together and the solution was stirred using a magnetic bar at 70ºC for two hours. Every 15 minutes the temperature of the solution was raised by 10ºC up to 130ºC. We got white viscous gel. The gel was placed in a preheated muffle furnace at 600ºC. At this temperature the solution evaporated, generating large amounts of gases, e.g. oxides of carbon and nitrogen. The combustion process lasted for about 5 to 10 minutes and resulted in white ash.

Fig. 1. $SrAl_2O_4$:Eu^{2+} nanosized powder synthesized by combustion method.

At the next step, the precursor was annealed at 1000^0 C for 1 and 2 hours under Ar /H_2 reductive atmosphere for the purpose reducing Eu^{3+} to Eu^{2+}.

X-ray diffraction patterns were recorded using a Bruker 5000 diffractrometer in standard θ-2θ geometry using Cu Kα radiation.

The luminescence spectra were detected using the UV-VIS-NIR (200-1700 nm) monochromator ARC SpectraPro-2300i equipped with Hamamatsu photon counting head H6240. All measurements were carried out in a liquid helium vacuum cryostat (5-400K temperature range, vacuum $2*10^{-7}$Torr) equipped with LakeShore 331 Temperature Controller. The cathodoluminescence measurements were performed under irradiation with electrons (5 keV, 0.4μA, spot»1mm^2).

3. RESULTS AND DISCUSSION

3.1 XRD analysis

X-ray diffraction (XRD) analysis was used to identify the crystal structure and phase purity of the pure and Eu doped $SrAl_2O_4$ phosphors.

It is clear from the XRD results that the main peaks in the sample due to $SrAl_2O_4$ and showing good consistence to the data from the standard powder diffraction file, JCPDS-01-024-11-87 [11]. But one of the intensive peak (32º) and also other peaks which are not coincide with this ICDD data have shown that it is a

131 H.Javid ave, AZ-1143, Baku
ANAS, G.M.Abdullayev Institute of Physics
E-mail: jophphysics@gmail.com

cubic phase $Sr_3Al_2O_6$ (a=b=c=15,844Å). But there are not any lines of combination of other elements. It means that all nitrates, boric acid and urea were dissolved and during 5-10 minutes the combustion process absolutely has finished.

3.2. CL measurements of $SrAl_2O_4:Eu^{2+}$.

First of all, it is still unclear whether the traps are related to host defects, the trivalent codopant, or a combination of both [8-10]. If host defects can play the role of traps then it could be useful for increasing duration of afterglow even without codopant.

In this paper CL measurements were carried out to study all observed peaks in detail. As the result of impinging high energy electrons, we can get detail information about peaks on PL spectrums [11]. Because of high energy electrons, we have observed a peak at 375 nm which was not clearly visible at FL spectrums at low temperatures.

First, it should be noted that the results of CL confirms the results of the spectrum FL [11].

Under VUV emission maximum peak at 520 nm and blue emission band at 442 nm were observed. The observed emission wavelength of 520 nm attributed to the $4f^65d^1 \rightarrow 4f^7$ transition of Eu^{2+} ion. The reason for the appearance of the blue band has been the subject of discuss for many years.

In addition were compared the results of CL of the Eu^{2+} doped and undoped $SrAl_2O_4$ and was determined that just two peaks (375, 250) nm were coincide (fig 3). It proves that these two peaks are not attributed to Eu^{2+} ion. This new peak at 375 nm can be attributed to crystal defects. The peak at 618 nm is presumably due to the emission of Eu^{3+} ions. The main reason to relate this peak to the second $Sr_3Al_2O_6$ phase is the observation of green band on the emission spectrum of $Sr_3Al_2O_6$ under UV excitation. Akiyama and coworkers [12-17] reported a green band on the emission spectra of $Sr_3Al_2O_6$: Eu under the excitation of 365 nm, which corresponds to our results. But XRD results [11] have shown that the concentration of this phase is low. So we can attribute this peak to the crystal defects within $SrAl_2O_4$.

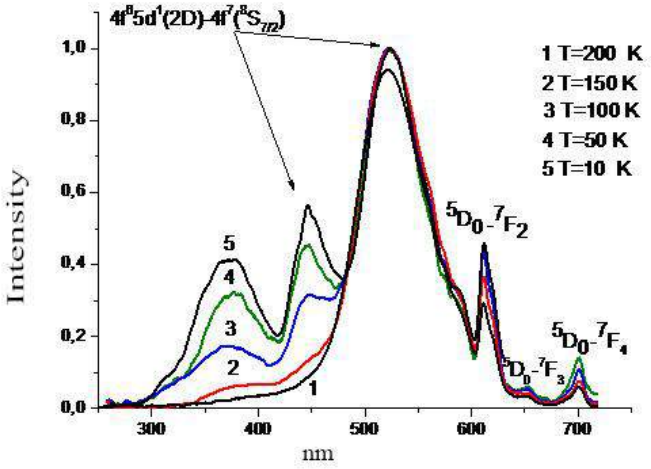

Fig.2. CL spectrums of $SrAl_2O_4$: Eu^{2+} nanophosphors at different temperatures

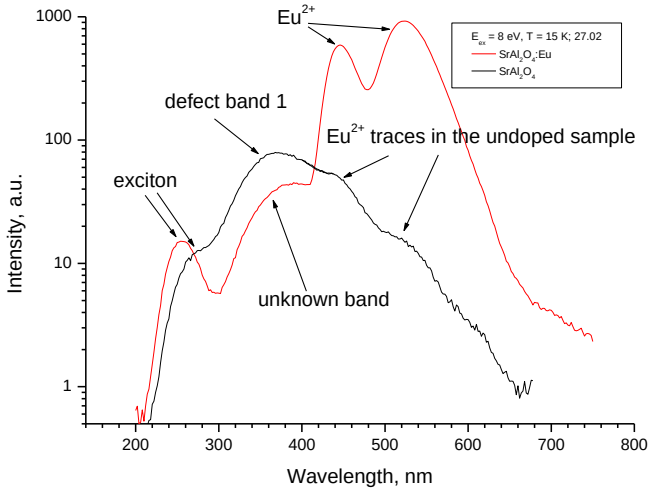

Fig 3. CL spectra of undoped and Eu doped $SrAl_2O_4$, E_{ex} = 8 eV, T = 15 K.

CONCLUSION

The nanosized green $SrAl_2O_4:Eu^{2+}$ phosphor was successfully synthesized by combustion synthesis. Cathodoluminescence properties at low temperatures are reported. Broadband VUV excited luminescence around 520 nm is attributed to $4f^65d \rightarrow 4f^7$ transition of Eu^{2+} ions in $SrAl_2O_4$. Another band at 450 nm was observed only at low temperature less than 150 K, and its nature is under discussion. New peak at 375 nm was observed and attributed to crystal defects within $SrAl_2O_4$.

[1] *C. Feldmann, T. Juestel, C. R. Ronda and P. J. Schmidt*, Adv. Funct. Mater., 13, 511, 2003.

[2] *J. HoËlsaË*, Electrochem. Soc. Interface, 18, 42, 2009.

[3] *M. Born and T. JuËstel*, Chem. Unserer Zeit, 40, 294, 2006.

[4] *G. Blasse, W.L. Wanmaker,; A. Bril*, Fluorescence of Eu2+ activated alkaline earth aluminates, *Philip. Res. Rep.* , *23*, 201, 1968.

[5] *J. Holsa, J. Hogne, M. Lastusaari, J. Niittykoski.* Persistent luminescence of Eu2+ doped alkaline earth aluminates MAl2O4:Eu2+, *J. Alloys Compounds*, *324*, 326,,2001.

[6] *S. Calyn, M. Nazarov, A. Nor Nazida and M. Ahmad –Fauzi* . Moldavian Journal of the Physical Sciences, 11,N1-2, 2012.

[7] Xibin Yu, Chunlei Zhou, Xianghong He, ZifeiPeng, Shi-Ping Yang. Materials Letters 58 1087, 2004.

[8] *P. Dorenbos*, J. Electrochem. Soc. **152**, H107, 2005.

[9] *F. Clabau, X. Rocquefelte, S. Jobic, P. Deniard, M. H. Whangbo, A. Garcia, and T. Le Mercier*, Chem. Mat. **17**, 3904, 2005.

[10] *T. Aitasalo, J. Hölsä, H. Jungner, J.-C. Krupa, M. Lastusaari, J. Legendziewicz, and J. Niittykoski*, Radiat. Meas. **38**, 727, 2004.

[11] *S.A. Mammadova, A.B. Hüseynov, T.Y. Orujov.* Azerbaijan Journal of Physics, v. XXI, N1, 2015.

[12] *M. Akiyama, C.-N. Xu, K. Nonuka, and T. Watanabe*: Appl. Phys. Lett.73 3046, 1998.

[13] *M. Akiyama, C.-N. Xu, M. Taira, K. Nonaka, and T. Watanabe*: Philos. Mag. Lett. 79, 735, 1999.

[14] *C. Kang, Ch. WenLi, X. Huang et. al.* Journal of Luminessence, , v.130, pp. 347-350, 2010.

[15] *P. Zhang, M. Xu, Z. Zheng, B. Sun, Y. Zhang*, Trans. Nonferrous Met. Soc. China 16 p. 423, 2006.

[16] *P. Zhang, L.X. Li, M.X. Xu, L. Liu*. J. Alloy Compd. 456, 1–2, 2008, 216.

[17] *P. Zhang, M.X. Xu, Z.T. Zheng, B. Sun, Y.H. Zhang.* Mater. Sci. Eng. B 136, 2007.

Received: 21.06.2016

ON THE CHARGE TRANSFER IN LAYERED SEMICONDUCTOR INDIUM SELENIDE

A.Sh. ABDINOV[1], R.F. BABAYEVA[2], E.A. RASULOV[1]
[1]Baku State University,
[2]The Azerbaijan State Economic University
Azerbaijan Republic, AZ 1145, Baku, Z. Khalilov Street, 23
Phone: (994 12) 5397373, e-mail: abdinov-axmed@yandex.ru,
abdinov_axmed@yahoo.com,
Babaeva-Rena@yandex.ru

At a variety of external and intracrystalline conditions experimentally studied electrical parameters and characteristics in the layered indium selenide semiconductor. A discussion of the results is made and the physical mechanism of found specific characteristics has been explained.

Keywords: crystal, doping, conductivity, a rare earth element, mobility of free charge carriers, Hall constant, drift barrier.
PACS: 71.20. Nr, 72.20.-i

1. INTRODUCTION

Often progress in fundamental and applied physics is determined by developments in the receipt and study of new semiconductor materials. As revealed at that theoretically unpredictable physical effects not only stimulate the development of the theory of semiconductors, but also the creation of fundamentally new functional elements for a variety of electronics industries.

Therefore, physicists and technologists continually conducted an intensive search in direction to prepare new semiconductor materials with specific structural features and a comprehensive study of varieties of their physical properties.

One of these materials is also indium monoselenide (InSe) belonging to the class of semiconductor compounds $A^{III}B^{VI}$ [1]. The peculiar (layered) crystal structure of this semiconductor gives it unique physical properties that for many years attracts attention of a wide circle of researchers various specialties.

To date the experimental study of the physical properties of InSe was the subject of many studies [-4], and in some cases has been found "unusual" features, i.e. they are not explained in the framework of theoretical ideas about physical properties of quasi-homogeneous crystalline semiconductors [5] and need for additional studies.

In the present paper we report about some of these "unusual" characteristics of the charge transport phenomena in *n*-InSe single crystals, received by us from comprehensive experimental studies of the effect of various external impacts and intracrystalline factors (doping, spatial heterogeneity, etc.) on their electrical parameters and characteristics. Naturally, such experimental studies, in addition to revealing the new features of this semiconductor, may also be useful to clarify the mechanism of various electronic effects also in other partially disordered crystalline semiconductors and identify new opportunities for their practical applications.

2. EXPERIMENTAL PROCEDURE AND SAMPLES

The investigated samples in the form of a rectangular parallelepiped with a thickness along the axis "C" (~ 300 μm) and lateral dimensions over the plane "C" (~ 2÷3x6÷8 mm) of the crystal cleaved from different portions of the same or different single crystalline ingots grown by slow cooling at constant gradient along the alloy [6]. Measurements were carried out in a wide range of temperatures (77- 450 K), intensity (E) of the external electric field (from extremely weak up to the switch voltage [4]). Pure and doped with rare earth elements (REE) samples were taken. As an impurity dysprosium, holmium and gadolinium were used. The doping was performed by introducing a desired quantity of the dopant in powder form into a batch before the synthesis process.

3. EXPERIMENTAL RESULTS

Studying the temperature dependence of the electrophysical parameters - specific conductivity (σ), the Hall constant (R_H) and the mobility of free charge carriers (μ) in *n*-InSe crystals it is found that in the temperature region below room temperature, conductivity (σ) of different samples differ depending on their technological origin. With decreasing temperature (T) from room temperature to liquid nitrogen temperature, R_H value is almost unchanged and has approximately the same numerical value for the different samples. In the crystals in which the value of σ at 77 K (initial specific conductivity value) not more than $10^{-4}\Omega^{1}\cdot cm^{-1}$, temperature dependence of σ and μ, unlike R_H, exhibit activation character, i.e. $\sigma,\ \mu \sim -\frac{\Delta\varepsilon}{kT}$ (fig. 1), where $\Delta\varepsilon$ - activation energy, k - Boltzmann constant.

The latter suggests that the observed at the low temperature region $\sigma(T)$ relationship in such (high resistance) crystals is not due to the temperature dependence of the concentration, and is associated with the dependence of the mobility of free charge carriers on the temperature.

131 H.Javid ave, AZ-1143, Baku
ANAS, G.M.Abdullayev Institute of Physics
E-mail: jophphysics@gmail.com

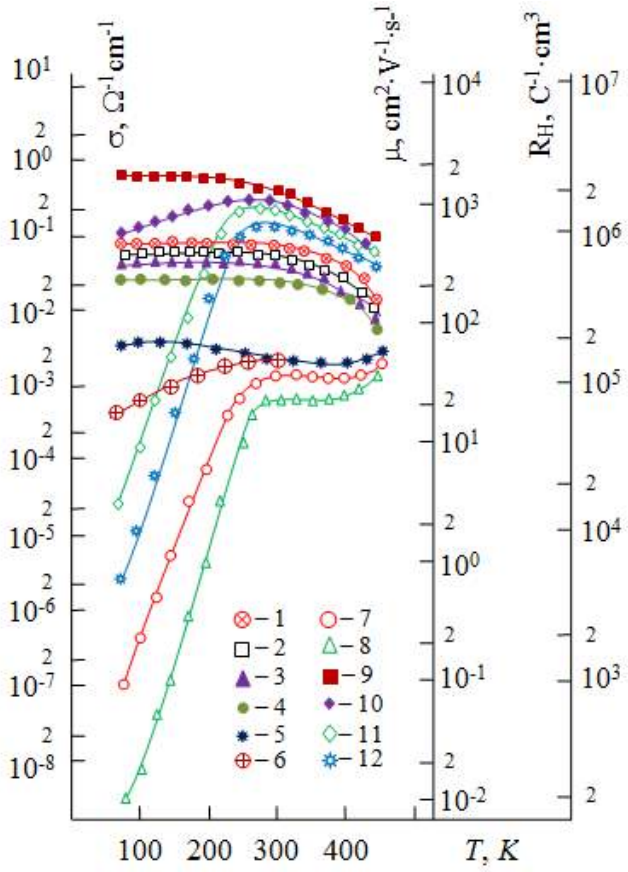

Fig.1. The temperature dependence of the Hall coefficient (R_H) (kr. 1-4), electrical conductivity (σ) (curves 5-8), and the mobility of free charge carriers (μ) (curves 9-12) in n-InSe crystals with different initial specific conductivity (σ_0): σ_0, $\Omega^{-1}\cdot cm^{-1}$: 1, 3, 5 - $2\cdot10^{-3}$; 2, 4, 6 - $2\cdot10^{-4}$; 7, 8, 9 - $2\cdot10^{-5}$; 10, 11, 12 - $6\cdot10^{-6}$.

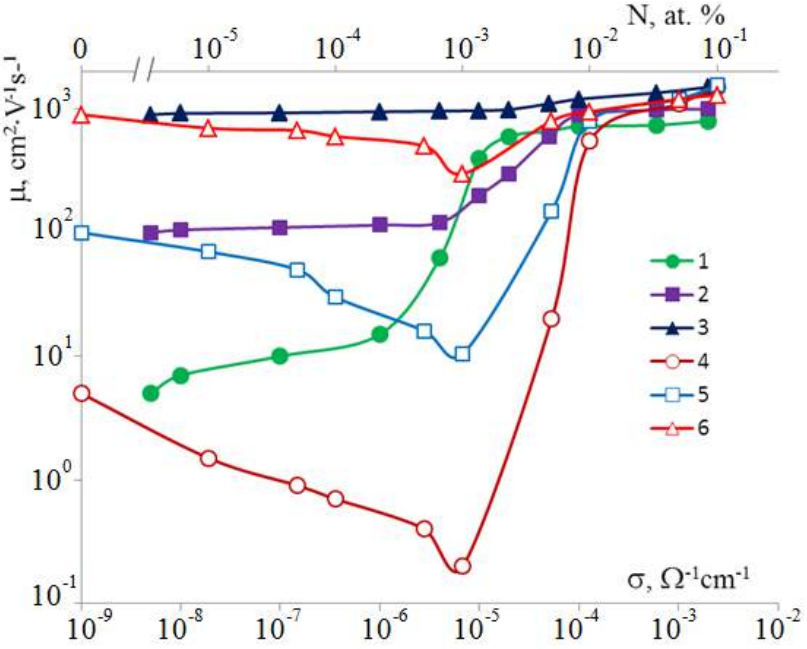

Fig.2. The dependence of the mobility of free charge carriers (μ) on the initial value of conductivity (σ_0) (curves 1-3) and the content of the introduced impurity (N) REE (curves 4-6) at different temperatures.
T, K: 1, 4 - 77; 2, 5 - 200; 3, 6 - 300.

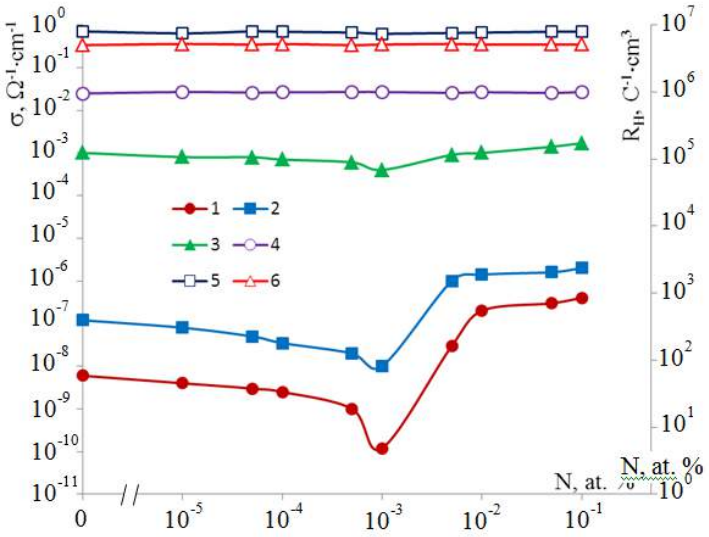

Fig.3. The dependence of the Hall coefficient (curves 1 to 3) and electrical conductivity (σ) (curves 4- 6) on the content of the introduced REE impurity (*N*) at different temperatures.
T, K: 1, 4 -77; 2, 5 - 200; 3, 6 - 300.

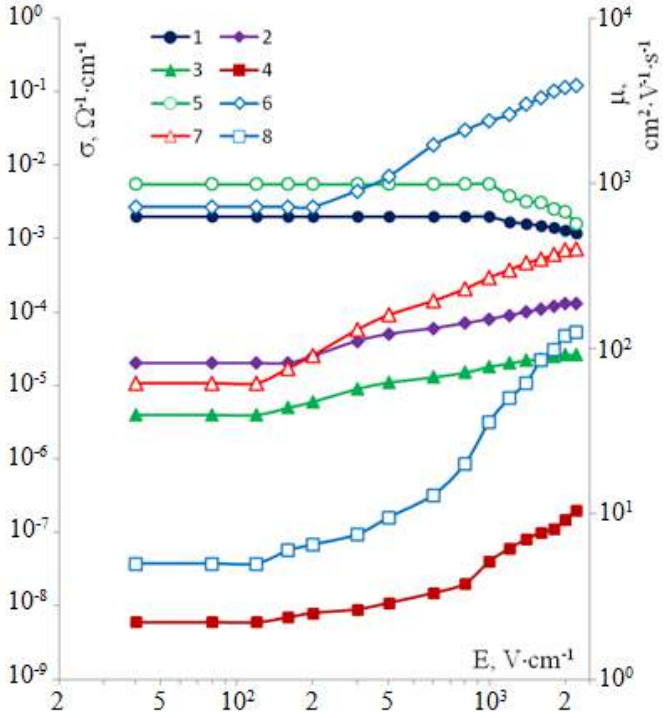

Fig.4. The dependence of specific conductivity (σ) (curves 1- 4) and mobility of free charge carriers (curves 5-8) on the electric field intensity (*E*) in pure (a) and doped with rare-earth elements (b) *n*-InSe crystals at 77 K.
a) σ_0, $\Omega^{-1}\cdot cm^{-1}$: 1, 5 – $2\cdot10^{-3}$; 2, 6 - $2\cdot10^{-5}$; 3, 7 - $4\cdot10^{-6}$; 4, 8 - $6\cdot10^{-7}$;
b) N, at. %: 1, 5 - 0; 2, 6 - 10^{-5}; 3, 7 - 10^{-3}; 4, 8 - 10^{-1}.

However, the experimentally observed dependence of $\mu(T)$ is not subject to the theoretical concepts of mobility of free charge carriers in quasi-ordered crystalline semiconductors [5].

At low temperature region were also found not characteristic for quasi-ordered crystalline semiconductors peculiarities for dependence of electrophysical parameters on doping (fig. 2 and 3) of the test specimen and on the impact of the external electric field (fig. 4). In particular, it was found that the value of μ in darkness at 77 K in low-resistivity crystals amounts up $1000\div1500 cm^2/V\cdot s$ and with decreasing σ to $5\cdot10^{-7}\Omega^{-1}\cdot cm$ decreases to parts per units.

In contrast to the low temperature region, at high temperatures $\mu(T)$ relationship obeys the law, which is characteristic for the mobility of free charge carriers in a quasi-ordered crystalline semiconductors with the dominance of the scattering of free charge carriers on acoustic lattice vibrations, i.e. $\mu \sim T^{-\frac{3}{2}}$ relationship is

observed (fig. 1). When other conditions being equal, with increase in the initial value of conductivity (σ_0) course of $\mu(T)$ curves approaches to predict by the theory for mobility of free charge carriers in quasi-ordered crystalline semiconductors. Effect of doping with rare earth elements on σ is observed only at low temperatures and at low doping levels ($N<10^{-2}$at.%). And it manifests itself both in changes of absolute value of μ and σ, and in the course of curves of dependences of these quantities on various external factors with N (fig. 2 and 3). It turned out that under considered by us conditions in the studied semiconductor values and characteristics of the electrophysical parameters are independent of the chemical nature of the introduced rare-earth impurity.

The specificity of the dependence of the charge transport from the influence of the external electric field (fig. 4) in *n*-InSe crystals is what, at that marked $\sigma(E)$ dependence starts to occur at relatively low values of E and has a very different character than predicted by corresponding theory for the dependence of the kinetic phenomena on E in the case of heating of free charge carriers in semiconductors by electric field [7].

4. DISCUSSION

We assume that found in high-pure and lightly doped with REE n-InSe crystals at measurements carried out by us specific (not explained in terms of theoretical concepts of the charge transport phenomena in quasi-ordered crystalline semiconductors) features of the charge transport is primarily associated with the presence in free bands of the semiconductor the drift and recombination barriers, with the original (taking place at 77 K) energy height for different samples ~ (0.05÷0.20) eV and ~(0.15÷0.40)eV. In favor of the validity of this assumption also testifies experimentally observed temperature dependence of the current density in these samples [3]. Detected at that dependence is associated with electrical erasing the drift barriers due to the implementation of a significant injection.

As for the whence of these barriers, first of all they can be caused by layered crystal structure of the semiconductor, segregation of its component atoms along the ingot during growth, as well as because of the variety of modifications [1].

5. CONCLUSIONS

The experimental results and their discussions lead to the following conclusions:

- When otherwise identical conditions the conductivity of individual samples of the layered n-InSe semiconductor single crystals in the low temperature region (T < 300 K) depends on technological origin of the examined sample;
- In high-resistivity ($\sigma_0 \leq 10^{-5}\Omega^{1}\cdot cm^{-1}$) crystals charge transport has specific (not explained by the theory of charge transport in a quasi-ordered crystalline semiconductors) features;
- These specific features of the charge transport in studied semiconductors directly related to the presence of the drift and recombination barriers in free bands of high-resistance crystals, as well as to control their parameters in different ways (temperature, doping, injection).

[1] *N.Kh. Abrikosov, V.F. Bankina, L.V. Poretskaya et al.* The semiconductor chalcogenides and their alloys. M. "Nauka", 1975, 219 p. (in Russian).

[2] *A.Sh. Abdinov, R.F. Babayeva*. Accumulation of the weak light signals memory and spectral memory in InSe<Dy> single crystals. Neorgan. Mater., 1995, v.31, n. 7, p. 896-898. (in Russian).

[3] *A.Sh. Abdinov, R.F. Babayeva.* Long-term isothermal relaxation of the dark resistivity of indium selenide single crystals doped with dysprosium. Neorgan. Mater., 1995, v.31, n. 8, p. 1020-1022. (in Russian).

[4] *A.Sh. Abdinov, R.F. Babayeva*. Switching effect in layered $A^{III}B^{VI}$ monoselenides and heterostructures on their basis. News of Baku University, 2009, n. 3, p. 139-147. (in Russian).

[5] *R. Smith.* Semiconductors, M., "Mir", 1991, 560 p. (in Russian).

[6] *A.M. Guseynov, T.I. Sadikhov*. Obtaining doped with the rare-earth indium selenide single crystals. In coll.: Electrical properties of semiconductors and gas discharge plasma. Baku. ASU, 1989, p. 42-44. (in Russian).

[7] *E. Conwell.* Kinetic properties of semiconductors in strong electric fields, M., "Mir", 1970, 384 p. (in Russian).

Received: 15.07.2016

FIRST PRINCIPLES CALCULATION OF THE VALENCE BAND OFFSETS FOR β- POLYTYPE OF A^3B^6 LAYERED CRYSTALS

Z.A. JAHANGIRLI[1,2]*, F.M. HASHIMZADE[1], D.A. HUSEYNOVA[1], B.H. MEHDIYEV[1], AND N.B. MUSTAFAYEV[1]

[1]Institute of Physics, National Academy of Sciences of Azerbaijan, Baku, Azerbaijan.
[2]Azerbaijan Technical University, Baku, Azerbaijan.

The valence band offsets (VBO) for the β-type A^3B^6 layered compounds depending on the thickness of the crystals have been investigated from the first principles, based on the density functional theory. To simulate the structure of a given thickness the periodic slab model was used. Two adjacent crystal slabs consisting of several layers were separated by a vacuum region of two-layer width. It is shown that at the crystal thickness more than 12 layers, photothreshold practically becomes independent on the thickness of the crystal.

Keywords: valence band offsets, DFT, photothreshold, slab model
PACS: 73.21-b, 73.40.Kp, 78.66.Fd, 79.60. Jv, 79.60.-i3

1. INTRODUCTION

Monochalcogenides GaS, GaS and InSe have a complex layered structure wherein each layer includes four alternating atomic planes X - M - M - X, where M = Ga, In, and X = S, Se. The unit cell of β-polytype these crystals contain two layers. The space group symmetry is P63/mmc (D_{6h}^4). All atoms are in the crystallographic position 4 (f): ± (1/3, 2/3, z) and ± (1/3, 2/3, 1/2-z). The lattice parameters and the positions of atoms in the structure in the fractional coordinates are follows: for GaS in the structure in the fractional coordinates are follows: for GaS a = 3.587 Å, c = 15.492 Å , z(Ga) = 0.1710, z(S) = 0.6016 [1]; for GaSe a = 3.742 Å, c = 15.919 Å, z(Ga) = 0.1748, z(Se) = 0.6018 [2]; for InSe a = 4.05 Å, c = 16.93, z(In) = 0.1570, z(Se) = 0.6020 Å [2] .

As shown in [3, 4], the ultrathin A^3B^6 crystals on various substrates can be used as a highly sensitive photodetectors. In addition, the above mentioned chalcogenides were found to be promising materials for the transformation of solar energy.

For determination of the VBO we calculated the photothreshold for each of above mentioned crystals. The photothreshold is the minimum energy required to remove an electron from the top of the valence band into the vacuum. Knowing the value of the photothreshold one can determine the contact potential difference in the hetero-structures used as solar energy converters. To the best of our knowledge there is only one study [5], where the photo thresholds of monolayer GaS, GaSe, and InSe were calculated from first principles. In this work have been calculated the valence band offsets (VBO) of these A^3B^6 crystals with various thicknesses. Results of the photothresholds calculations for the monolayer A^3B^6 crystals are also included for comparison with the results of the theoretical calculations of [5].

2. CALCULATION METHOD

To simulate the structure of a given thickness the periodic slab model was used. Our estimation shows that the vacuum thickness of about 18 Å is sufficient for interactions between adjacent slabs to be neglected. Actually, we have constructed a super-lattice of one, two or more unit cells of A^3B^6 crystal with the vacuum of one unit-cell-thick.

The calculations have been carried out from first principles using the plane wave pseudopotential code ABINIT [6]. Exchange correlation interaction was described in the local density approximation (LDA) according to [7]. The numerical integration over the Brillouin zone was carried out using the Monkhorst-Pack 12×12×1 grid with the (0, 0, 0.5) shift from the origin [8]. For the pseudopotentials we use the norm-conserving Hartwigsen – Goedecker - Hutter pseudopotentials [9]. In the wave function expansion we included the plane waves with the maximal energy up to 1350 eV, which ensures good convergence of the total energy. The atomic positions and structural parameters have been optimized by calculating the Hellmann-Feynman forces. The equilibrium parameter values were determined by minimization of the total energy with precision of up to 10-6 eV per unit cell. The modules of forces are minimized with the criterion of 10-4 eV/Å.

3. DISCUSSION OF THE RESULTS

The analysis of calculated equilibrium positions of atoms (Table 1-3) show that the structural change of slabs, consisting of multiple layers is insignificant. This is not surprising as the interlayer interaction in these crystals is weak, and distant layers have little effect on the geometry of the surroundings of atoms in the particular layer. The tables 1-3 also show the thickness and vacuum settings for monolayers of [5].

The dependencies of the value of the photothreshold on the thickness of GaS, GaSe, and InSe are shown in fig.1. The value of the photothreshold correspond to the energy difference between the electrostatic potential in a vacuum region far from the neutral surface of crystal and the Fermi level which coincides with the top of the valence band in this case.

In [5] for the monolayer of the A^3B^6 crystals, a more accurate hybrid functional was used to calculate more precise absolute valence band maximum positions. In our calculations ordinary DFT method have been used, whose limitations are well known to accurately predict excited-state properties, band gap and absolute energy positions of the valence band maximum.

Nevertheless, we found that (Tab. 4) the energy difference between the valence band maxima of the various compounds of this monochalcogenides group quite close to the results obtained by a more advanced method used in [5].

131 H.Javid ave, AZ-1143, Baku
ANAS, G.M.Abdullayev Institute of Physics
E-mail: jophphysics@gmail.com

Table 1.

Equilibrium values of the parameters of crystal structure of GaS for various thicknesses

Number of layers	Lattice parameter (Å)	Interatomic distances (Å)		Layer thickness (Å)	Crystal thickness (Å)	Interlayer distance (Å)	Vacuum width (Å)
	a	d_{Ga-Ga}	d_{Ga-S}				
1*	3.58	2.45	2.33			-	18
1	3.487	2.36	2.27	4.47	4.47	-	25.74
2	3.489	2.36	2.27	4.47	12.04	3.096	18.30
4	3.49	2.36	2.27	4.47	27.18	3.096	18.44
6	3.49	2.36	2.275	4.47	42.32	3.096	18.22
8	3.49	2.36	2.275	4.47	52.99	3.096	18.41
10	3.49	2.36	2.275	4.47	72.60	3.097	18.24
12	3.49	2.36	2.28	4.47	87.74	3.10	18.24

Note: 1* are taken from [5].

Table 2.

Equilibrium values of the parameters of crystal structure of GaSe for various thicknesses

Number of layers	Lattice parameter (Å)	Interatomic distances (Å)		Layer thickness (Å)	Crystal thickness (Å)	Interlayer distance (Å)	Vacuum width (Å)
	a	d_{Ga-Ga}	d_{Ga-Se}				
1*	3.75	2.44	2.46			-	18.00
1	3.66	2.35	2.40	4.64	4.64	-	26.71
2	3.67	2.35	2.41	4.64	12.47	3.20	18.87
4	3.67	2.35	2.41	4.64	28.13	3.19	18.87
6	3.67	2.35	2.41	4.64	43.79	3.19	18.86
8	3.67	2.35	2.41	4.64	59.48	3.19	18.84
10	3.67	2.35	2.41	4.64	75.11	3.19	18.84
12	3.67	2.35	2.41	4.64	90.77	3.19	18.84

Table 3.

Equilibrium values of the parameters of crystal structure of InSe for various thicknesses

Number of layers	Lattice parameter (Å)	Interatomic distances (Å)		Layer thickness (Å)	Crystal thickness (Å)	Interlayer distance (Å)	Vacuum width (Å)
	a	d_{In-In}	d_{In-Se}				
1*	4.02	2.77	2.65			-	18
1	3.90	2.66	2.57	5.15	5.15	-	27.57
2	3.91	2.67	2.57	5.15	13.32	3.03	19.39
4	3.91	2.67	2.58	5.14	29.66	3.02	19.36
6	3.91	2.67	2.58	5.14	46.00	3.03	19.37
8	3.91	2.67	2.58	5.14	62.34	3.02	19.38
10	3.91	2.67	2.58	5.14	78.61	3.02	19.39
12	3.91	2.67	2.58	5.15	95.10	3.02	19.40

Table 4.

Calculated valence band offset (VBO)
for monolayers of GaS, GaSe, and InSe.

Crystal contact	VBO (eV)	VBO[a] (eV)
GaSe/GaS	0.39	0.41
GaSe/InSe	0.14	0.15
InSe/GaS	0.25	0.26

[a]Ref.[5]

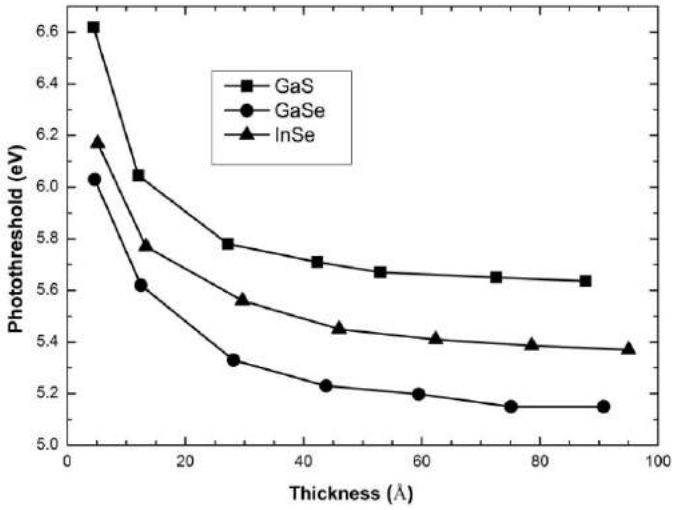

Fig. 1. Photothreshold as a function of the thickness of GaS, InSe, GaSe crystals.

We believe that this situation takes place for arbitrary thickness of monochalcogenides crystals of gallium and indium. Thus, the results of our calculations can be used to calculate the contact potential difference of these crystals. In particular, we found that the difference between the maxima of the valence bands of GaSe and InSe with large thicknesses is about 0.2 eV, which is close to the values estimated from the experiments on electron diffraction, X-ray photoelectronic spectroscopy [11], and electroluminescence [12].

4. CONCLUSION

This is first report of ab initio local density functional calculations of the thickness dependences of the valence band offsets of β-polytype monochalcogenides GaS, GaSe, and InSe. The method of periodic slabs separated by vacuum of two-layer width was used to model a finite thickness of a crystal. It has been shown that the valence band offsets are practically independent of the crystal thickness when the latter exceeds 12 layers.

[1] *A. Kuhn, A. Chevy, R. Chevalier.* Acta Cryst. 32, 983, 1976.
[2] *R.W.G. Wyckoff.* Crystal Structures, Second edition. Interscience Publishers, New York, 1, 237. 1963.
[3] *P.A. Hu, L. Wang, M. Yoon, J. Zhang, W. Feng, X. Wang, Z. Wen, J .C. Idrobo, Y. Miyamoto, D.B. Geohegan, K. Xiao.* Nano Lett. 13,1649, 2013.
[4] *J. Martínez-Pastor, A. Segura, J. Valdes, A. Chevy.* J. Appl. Phys. 62, 1477, 1987.
[5] *H.L. Zhuang, R.G. Hennig.* Chem. Mater. 25, 3232 2013.
[6] *X. Gonze, B. Amadon, P.M. Anglade, J.M. Beuken, F. Bottin, P. Boulanger, F. Bruneval, D. Caliste, R. Caracas, M. Cote, T. Deutsch, L. Genovese, Ph. Ghosez, M. Giantomassi, S. Goedecker, D.R. Hamann, P. Hermet, F. Jollet, G. Jomard, S. Leroux, M. Mancini, S. Mazevet, M.J.T. Oliveira, G. Onida, Y. Pouillon, T. Rangel, G.M. Rignanese, D. Sangalli, R. Shaltaf, M. Torrent, M.J. Verstraete, G. Zerah, J.W. Zwanziger.* Comp. Phys. Comm. 180, 2582, 2009.
[7] *S. Goedecker, M. Teter, J. Hutter.* Phys. Rev. B 54, 1703, 1996.
[8] *H.J. Monkhorst, J.D. Pack.* Phys. Rev. B 13, 5188, 1976.
[9] *C. Hartwigsen, S. Goedecker, J. Hutter.* Phys. Rev. B 58, 3641, 1998.
[10] *J. Heyd, G.E. Scuseria, M. Ernzerhof.* J. Chem. Phys. 118, 8207, 2003.
[11] *O. Lang, A. Klein, C. Pettenkofer, W. Jaegermann, A. Chevy.* J. Appl. Phys. 80, 3817, 1996.
[12] *N. Balakrishnan, Z.R. Kudrynskyi, M.W. Fay, G.W. Mudd, S.A. Svatek, O. Makarovsky, Z.D. Kovalyuk, L. Eaves, P.H. Beton, A. Patane.* Adv. Optical Mater. 2, 1064, 2014.

Received: 12.07.2016

MODELLING THE INFLUENCE OF THE MELTING ZONE LENGTH ON COMPONENT CONCENTRATION DISTRIBUTION IN Ge-Si CRYSTALS GROWN BY MODIFIED MELTING ZONE METHOD

Z.A. AGAMALIYEV[1,2], M.A. RAMAZANOV [2], G.H. AJDAROV[1]
[1]Institute of Physics of Azerbaijan NAS
AZ-1143, H.Javid ave., 131
phone:(+99412)5393218, Fax: (+99412)4395961
[2]Baku State University
AZ 1148, Baku, Z.Khaslilov str., 23
zangi@physics.ab.az

The problem of component concentration axial distribution of Ge-Si crystal solid solutions grown by modified zone melting method using the germanium seed is solved in completely mixed melt approximation.

The axial concentration profiles of components in crystals grown at different melting zone lengths are calculated taking into consideration the complicated dependence of silicon segregation coefficient on melt composition. The possibility of control of component concentration distribution in Ge-Si crystals in wide range by way of change of melting zone length is shown. The analysis of obtained results determines the optimal technological parameters for growing Ge-Si crystal solid solutions with given homogeneous and heterogeneous compositions along matrix.

Keywords: Ge, Si, solid solutions, Pfann approximation, melting zone, component distribution.
PACS: 81.10.Aj.

INTRODUCTION

The preparing of the material with given component concentration distribution in matrix and support of its monocrystallinity is the main problem of bulk crystal growth process of semiconductor solid solutions from the melt. The classic system Ge-Si the composite components of which are the basis materials of modern micro- and optoelectronic industry takes the dominant place in series of semiconductor solid solutions. The silicon and germanium totally solve in each other in any ratios in both liquid and solid states and form the continuous series of exchange solid solutions [1,2].

The mathematical modeling the concentration component profile along Si-Ge crystals grown by modified zone recrystallization method using germanium seed is carried out in Pfann approximation in the present paper. The aim is the potential determination of the modified method for obtaining of bulk Ge-Si single crystals with the given axial component concentration distribution.

THE THEORETICAL BASIS AND MODELING THE COMPONENT DISTRIBUTION IN Ge-Si CRYSTALS

The tasks on modeling the component concentration profiles in Ge-Si crystals grown from the melt by series of conservative and non-conservative methods were solved earlier in works [3-10], the results of which showed the well agreement with experimental data.

The conceptual scheme of crystal growing of solid solutions by modified method of zone melting is presented in fig.1.The monocrystalline seed (1) from Ge (fig.1A) is put into crucible of cylindric form. The previously prepared rods of definite diameter from germanium (2) and Ge-Si macro-homogeneous solid solution with the given composition (3) are put under the seed. The rod melting (2) from Ge situated directly under the seed (fig.1B) is carried out in vacuum conditions. The temperature on the melt boundaries with the seed and ingot is equal to germanium melting point in restarting moment of recrystallization. The crystal growth takes place on the seed from the moment of switching on of crucible movement mechanism relatively heater and continues up to total ingot recrystallization (3). Its length is kept constant and equal to Z up to the moment of formation of final zone. Here the initial melting zone consists in the pure germanium in difference on traditional method of zone melting [2,11]. This circumstance solves the seed problem necessary for growing up of Ge-Si solid solutions single crystals of different composition by the way of germanium seed usage.

The task of concentration distribution of silicon and germanium atoms along Si-Ge crystal grown up by modified method of zone melting is solved in Pfann approximation at carrying out of the following standard conditions [11]: the component diffusion in solid phase is negligible one; the crystallization front is plane one; the equilibrium between liquid and solid phases is on the crystallization front; the diffusion rate of Si and Ge atoms in the melt provides its homogeneity along whole volume (totally mixed composition); the segregation coefficients of melt components change with its composition in correspondence with diagram of equilibrium phase state of Si-Ge system; thermal expansion or compression of material at phase transitions is negligible one; the composition of Ge-Si initial ingot is macro-homogeneous one.

Let's introduce the following designations: C_c , C_i , C_m are atomic fraction of second component (Si) in the crystal, initial polycrystalline rod and melt correspondingly; C is Si general atomic fraction in the

131 H.Javid ave, AZ-1143, Baku
ANAS, G.M.Abdullayev Institute of Physics
E-mail: jophphysics@gmail.com

melt; C_m^0 is Si atomic fraction in melting zone in initial moment; V_c is melt volume crystallizing in time unit; V_i is Ge-Si initial ingot volume melting in time unit; V_m^0 and V_m are volumes of melting zone in initial and current moments; $K = C_c/C_m$ is Si equilibrium segregation coefficient; L is total length of initial rods from Gre and Ge-Si; ℓ is length of material recrystallized part in *t* moment; Z is melting zone length.

In frameworks of introduced designations we have the following:

$$C_m = \frac{C}{V_m};\ \frac{dC_m}{dt} = \frac{\dot{C}V_m - \dot{V}_m C}{V_m^2};$$
$$V_m = V_m^0 - (V_c - V_i)t\ ; \qquad (1)$$

By problem situation, Z, V_i and V_c parameters don't depend on time up to formation of final melting zone. In this case the following ratios are equal on the section by L-Z-length from the seed (see fig.1A and 1C) in process of zone crystallization:

$$V_m = V_m^0\ ;\quad V_i = V_c;\ C_m^0 = 0 \quad \text{and}$$
$$\dot{C} = V_i C_i - V_c C_m K \qquad (2)$$

Substituting (2) into (1) after series of transformations and integration, we have:

$$\int_0^{C_m} \frac{dC_m}{C_i - C_m K} = \frac{V_c t}{V_m^0} = \frac{l}{Z} \qquad (3)$$

Taking into consideration the equality $K = C_c/C_m$ the equation (3) confirms the component part composition along the length of growing crystal on section from ℓ =0 up to ℓ = L-Z. In final section the following ratios are from the moment of final melting zone formation by Z length.

$$V_i = 0,\quad V_m = \mathrm{V_m^0} - \mathrm{V_c}t,\quad \dot{V}_m = -V_c,$$
$$\dot{C} = -V_c\ C_m K \qquad (4)$$

Taking into consideration (4) after series of transformations and integration we have:

$$\int_{C_{mf}^0}^{C_m} \frac{dC_m}{C_{mf}^0 - C_m k} = \ln \frac{V_m^0}{V_m^0 - V_c t} \qquad (5)$$

Here C_{mf}^0 is start concentration part of Si atoms in the melt in final melting zone formation moment. Introducing the length and crystallized part of melt final part ($V_c t/V_m^0$) in t moment by l^* and γ symbols correspondingly let's write the equation (5) in the following form:

$$\gamma \equiv \frac{l^*}{Z} = 1 - \exp\left[- \int_{C_m}^{C_{mf}^0} \frac{dC_m}{C_m K - C_m} \right] \qquad (6)$$

The confirmation of l/Z and γ as C_m (also as $C_c = K\ C_m$) function along whole material length treated by zone crystallization requires the integral solutions in equations (3) and (6). The segregation coefficient of second component (*K*) including in both these equations enough difficultly depends on C_m [7,8]. This circumstance leads to necessity of calculation of integrals in (3) and (6) by numerical method with the use of diagram data of Ge-Si system equilibrium phase state. In recent paper [4] it is shown that the temperatures of $T_l(C_m)$ liquids and $T_s(C_m)$ solidus curves of system diagram state in whole C_m change interval from) up to 1 are well enough described by following polynomials of fifth degree:

$$T_l(C_m) = 938.72\ ^0C + p_1 C_m + p_2 (C_m)^2 + p_3 (C_m)^3 + p_4 (C_m)^4 + p_5 (C_m)^5 \qquad (7)$$

$$T_s(C_m) = 938.72\ ^0C + q_1 C_m + q_2 (C_m)^2 + q_3 (C_m)^3 + q_4 (C_m)^4 + q_5 (C_m)^5 \qquad (8)$$

Here 938.72 ^{0}C is Ge melting point:
$p_1 = 1.523764 \times 10^3$, $p_2 = -3.893151 \times 10^3$,
$p_4 = -6.011559 \times 10^3$, $p_5 = 2.007591 \times 10^3$,
$q_1 = 2.449722 \times 10^2$, $q_2 = 3.29571 \times 10^2$,
$q_3 = -8.419889 \times 10^2$, $q_4 = 1.543233 \times 10^3$,
$q_5 = -8.023673 \times 10^2$.

The absolute error in $T_l(C_m)$ and $T_s(C_m)$ numerical values in whole temperature interval doesn't exceed 1.69 ^{0}C and 0.39 ^{0}C correspondingly. The equations (7) and (8) give the possibility to confirm C_c and $K = C_c/C_m$ values conjugated with the given C_m with enough degree of accuracy. Introducing C_m values gradually in the required interval and confirming *K* values conjugated with them, the integrals in (3) and (6) are solved by numerical method.

The character curves of silicon concentration distribution along Ge-Si crystals for different Z values calculated from equations (3) and (6) with taking into consideration $C_c = C_m K$ are presented on fig.2.

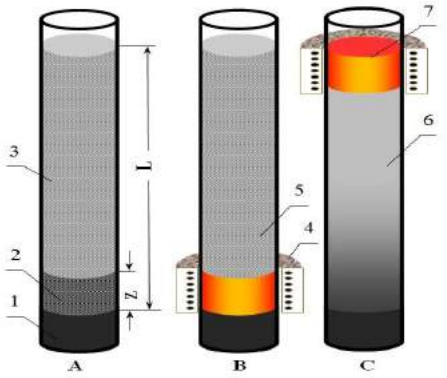

Fig.1. The scheme of growing up of Ge-Si solid solution single crystals by zone melting method with the use of germanium seed. A is order of crucible loading: 1, 2 are seed and rod from Ge; 3 is Ge-Si macrohomogeneous rod of the given composition; B is crystallization start position: 4 is heater, 5 is melt from Ge; C is the moment of final melting zone formation: 6 is Ge-Si single crystal, 7 is Ge-Si melt; L and Z are the lengths of the given sections.

In calculations the start compositions of all initial macro-homogeneous rods is equal to $Ge_{0.7}Si_{0.3}$.

As it is seen from this figure Z operating parameter significantly influences on component redistribution at zone recrystallization of Ge-Si initial rod of the given composition. Moreover, the lengths of both homogeneous and heterogeneous parts of the crystal are confirmed by Z value of melting zone. The family of curves (fig.2) visually demonstrates the potential and availability of modified method of zone melting for obtaining of Ge-Si solid solution single crystals with required homogeneous and alternative compositions by the way of selection of corresponding values of technological parameters (Z, C_i).

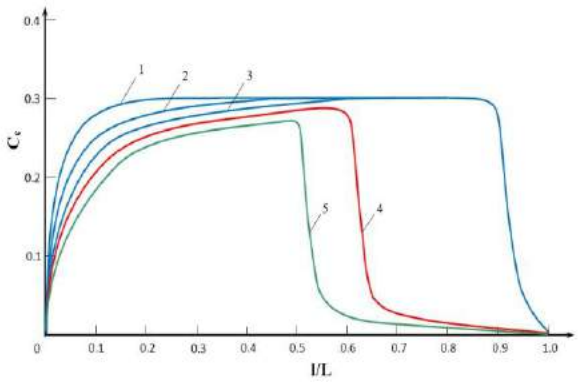

Fig.2. Si calculative concentration profiles along Ge-Si single crystals grown up by modified method of zone melting at different values of Z melting zone. The curves 1,2,3,4,5 correspond to values Z/L= 0.1, 0.2, 0.3, 0.4, 0.5 correspondingly. The composition for all initial ingots of solid solutions is equal to $Ge_{0.7}Si_{0.3}$

CONCLUSION

Summarizing the above mentioned, one can conclude the following. The math modeling of axial component distribution in Ge-Si crystals grown up by modified method of zone recrystallization, carried out with taking into consideration the difficult character of component segregation coefficient change with melt composition gives the possibility to carry out the estimation of optimal technological parameters (melting zone length and initial composition of feeding rod) for obtaining of solid solution crystals with the given component concentration profile.

[1] *V.S. Zemskov, V.B. Lazerov.* Tverdie rastvori v poluprovodnikovix sistemax. «Nauka», Moskva, 1978, 197. (In Russian)

[2] *J. Schilz, V.N. Romanenko.* Bulk growth of Silicon-Germanium Solid Solutions, J. Materials in Electronics,V.6, 1995, 265-279

[3] *G.Kh. Azhdarov, T. Kucukomeroglu, A. Varilci et al.* Distribution of components in Ge-Si bulk single crystals grown under continuous feeding of the melt with the second component (Si), J. Crystal Growth, 226, 2001, 437-442

[4] *I. Kostylev, J.K. Woodacre, Y.P. Lee et al.,* Melt zone growth of Ge-rich $Ge_{1-x}Si_x$ bulk single crystals, J. Crystal Growth, 377, 2013, 147-157

[5] *T.A. Campbell, M. Schweizer, P.Dold et al.*. Float zone growth and characterization of $Ge_{1-x}Si_x$ (x<10 at. %) single crystals, J. Crystal Growth, 226, 2001, 231-237

[6] *N.V.Abrosimov, S.N. Rossolenko, Thieme W. et al.*. Czochralski growth of Si- and Ge-rich Si-Ge single crystals, J. Crystal Growth, 174, 1997, 182-186

[7] *Z.M. Zaxrabova.* Kristalli tverdix rastvorov Ge-Si. Poluchenie i elektricheskie svoystva slojnoleqirovannix kristallov Ge-Si s primesyami medi, alyuminiya i surmi, LAP LAMBERT Academic Publishing, Germaniya. 2013, 139. (In Russian)

[8] *V.K. Kazimova.* Kristalli Ge-Si I ix svoystva. Poluchenie i elektricheskie svoystva tverdix rastvorov Ge-Si, slojnoleqirovannix primesyami medi, indiya i surmi, LAP LAMBERT Academic Publishing, Germaniya. 2013, 144. (In Russian).

[9] *G.Kh. Azhdarov, R.Z. Kyazimzade,* Growth of homogeneous single crystals of Ge-Si solid solutions by the modified Bridgman method, Crystallography Reports, 50, 2005, S149-S153

[10] *G.Kh. Azhdarov, Z.M. Zeynalov, Z.A. Agamaliyev, A.I. Kyazimova.* Growth of single crystals of semiconductor solid solutions by double feeding of the melt method, Crystallography Reports, 55, 2010, 763-767

[11] *V.B. Qlazov, V.S. Zemskov.* Fiziko-ximicheskie osnovi leqirovaniya poluprovodnikov. M.: Nauka, 1967, 371. (In Russian)

Received: 20.05.2016

THE INVESTIGATION OF NONLINEAR ABSORPTION OF LASER BEAMS IN DIFFERENT OIL SAMPLES

G.T. GASANOV, M.A. MUSAYEV, A.N. JAFAROV, N.N. GASHIMOVA
Azerbaijan State University of Oil and Indutsry
AZ 1010, Baku, Azdaligave., 20, aymin@mail.ru

The appearance and distribution of optoacoustic signal in different oil samples are experimentally investigated. The bond between absorption coefficient and period of acoustic signal is established. The confirmation technique of nonlinear absorption coefficient of laser beams in liquids is suggested.

Keywords: nonlinear absorption, optoacoustic signal, oil.
PACS: 42.65.

INTRODUCTION

The nonlinear optic effects at interaction of light with liquids present the big interest for both the study of their fundamental properties and investigation of possibilities of their practical use in different fields of science and technique. In connection with the fact that experimental and theoretical investigations of non-linear one- and multi-photon absorption and also other nonlinear optical effects in liquids which haven/t been studied yet, the revealing of their coexistence or competition, domination or redistribution of the influence at different excitation conditions present the big scientific interest.

There are two main reasons causing the different character of light field interaction of low and big intensity with the substance. Firstly, the multi-photon processes play the main role at high intensity besides the one-photon processes confirming the interaction on microscopic level at low light intensity. This means that not one but several phonons are absorbed in light interaction elementary act with substance atom. Secondly, the substance initial properties under the light influence propagating in it change at big intensity. The substance characteristics become alternative values depending on incident light intensity, i.e. the medium becomes nonlinear. As a result the dependence of optical phenomenon character on light intensity value appears. Consequently, the interaction has the nonlinear character at big intensity in difference from interaction linear character belonging to low intensity light.

The appearance and distribution of optoacoustic waves in oil and oil products are experimentally investigated in [1,2]. The increase of technological process efficiency with the help of physical field influence has had the important practical use last time. In particular, the treatment by laser beams should lead to increase of transmission capacity of oil products at transportation of oil and oil products. In this connection the investigation necessity of nonlinear interaction of laser beams with oil samples appears.

EXPERIMENTAL INSTALLATION AND INVESTIGATION TECHNIQUE

The laser facility (fig.1) the principle of operation of which is described in [3], is used at carrying out of investigations. TEA CO_2 impulse laser working on wave length 1,06 μm serves as the optical radiation source. The duration and laser impulse energy are 20nsec and 5MJ correspondingly. The unfocused beam of laser radiation by diameter 1,6 cm is vertically directed to cell with investigated liquid. The experiments show that optoacoustic signal front for all investigated oil samples by the form is similar. The heterogeneity of temperature and absorption coefficient confirms the form of optoacoustic signal. In the given case all experiments are carried out at the similar temperature. By this reason the difference of wave front of optoacoustic signals in different oil samples is confirmed by the difference of oil absorption coefficient.

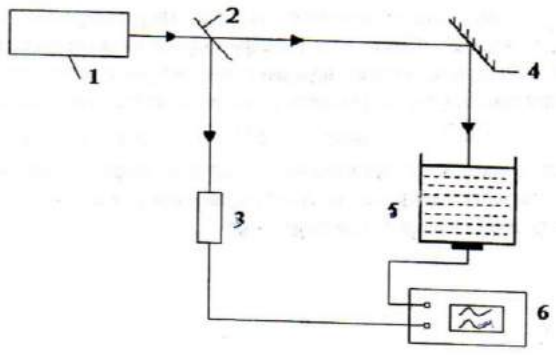

Fig.1. The scheme of experimental installation for investigation of liquid optoacoustic properties (1 is impulse laser CO_2, 2 is semitransparent plate, 3 is photodetector, 4 is mirror, 5 is cell with investigated oil, 6 is oscillograph by C9-8 type).

The optoacoustic signal form for three oil samples is shown on fig. 2.

Carrying out the treatment of experimental data in Matlab medium it is established that these curves of optoacoustic pressure distribution in dependence on time can be described by the formula:

$$P(t) = At^n \exp(-Bt^2) \qquad (1)$$

Here B coefficient characterizes the absorption coefficient. It is seen that the optoacoustic pressure shifts to the side of big t with increase of absorption coefficient, i.e. both the period and amplitude of oscillations increase with absorption coefficient increase.

131 H.Javid ave, AZ-1143, Baku
ANAS, G.M.Abdullayev Institute of Physics
E-mail: jophphysics@gmail.com

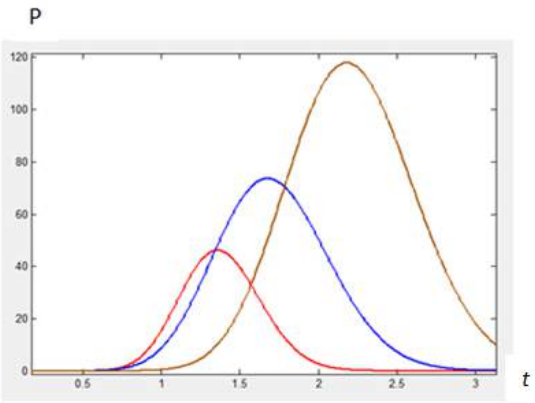

Fig. 2. The graph of *P* optoacoistic pressure dependence on t time. The samples are taken from Shievan, Garadag and Binagadi oilfields.

The connection between oscillation period and absorption coefficient is confirmed by us from the condition of curve maximum:

$$\frac{T^2 B}{n} = 8 \qquad (2)$$

B, *n*, *A* and *t* including in (1) is presented in table:

B	3,86	1,93	1,54
n	14,2	10,87	14,59
A	739,5	61,16	2,02
t_{max}	1,35	1,68	2,78

The wave leading front is the information part of optoacoustic signal. The non-linear factor of second order can be confirmed by signal information part character, i.e. signal front character.

THE RESULTS AND DISCUSSION.

Let's consider the non-linear interaction of laser beams with liquid at multi-photon absorption. At non-linear interaction of laser beams with liquid the intensity change with thickness is expressed by the formula:

$$-d\dot{I} = \alpha \dot{I} dx + \delta_n \dot{I}^n dx \qquad (3)$$

Neglecting the linear absorption (one-photon absorption) from (3) we have:

$$\dot{I} = \frac{\dot{I}_0}{\left(1+(n-1)\delta_n \dot{I}_0^{n-1} x\right)^{\frac{1}{n-1}}}, \dot{I}(0) = \dot{I}_0 \qquad (4)$$

Moreover, the optoacoiustic pressure is confirmed by formula:

$$P_n = \frac{1}{2c_p} \frac{c_0^2 \beta \delta_n \dot{I}_0^n}{\left(1+(n-1)\delta_n \dot{I}_0^{n-1} x\right)^{\frac{n}{n-1}}} \qquad (5)$$

The optoacoustic pressure appearing at linear interaction of laser beams with liquid is expressed by formula:

$$P_1 = \frac{\alpha c_0^2 \beta \dot{I}_0}{2c_p} e^{-\alpha x}, \qquad (6)$$

From comparison of (5) and (6) formulae we have:

$$\frac{P_1}{P_n} = \frac{e^{-\xi}}{\sigma_n}\left[1+(n-1)\sigma_n \xi\right]^{\frac{n}{n-1}}, \qquad (7)$$

where $lx=\xi$ and $\sigma_n = \frac{\gamma \dot{I}_0^{n-1}}{\alpha}$. The graph of $\frac{P_1}{P_n}$ dependence on ξ at different σ_n and *n* values is shown on fig.3.

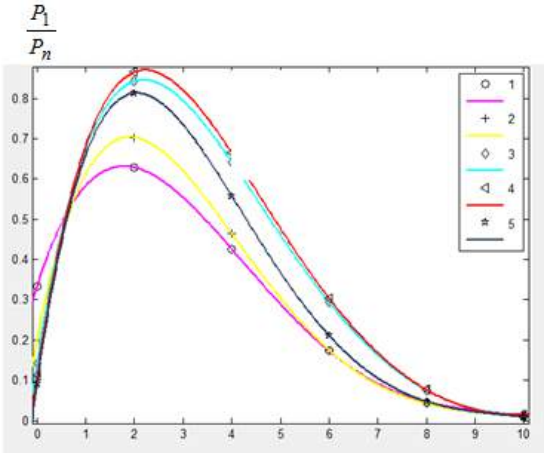

Fig.3. The graph of $\frac{P_1}{P_n}$ dependence on ξ at σ different values.

Formula (7) allows us to confirm the nonlinearity coefficient of *n* order. For this aim let's logarithm the formula (7):

$$\ln \frac{P_1}{P_n} = -\xi - \ln \sigma_n + \frac{n}{n-1} \ln\left[1+(n-1)\sigma_n \xi\right] \qquad (8)$$

From (8) it follows that at ξ=0, $\ln \frac{P_1}{P_n} = -\ln \sigma_n$

From here

$$\frac{P_1}{P_n} = \frac{1}{\sigma_n} = \frac{\alpha}{\delta_n \dot{I}_0^{n-1}} \qquad (9)$$

The non-linearity coefficient of *n* order can be confirmed from (9) on the base of experimental data knowing $\frac{P_1}{P_n}$:

$$\delta_n = \frac{\alpha}{\dot{I}_0^{n-1}} \frac{P_n}{P_1} \qquad (10)$$

Taking into consideration that one- and multi-photon absorption of laser beams in liquids take place simultaneously and applying the superposition principle we have the following expression for resulktant pressure of optoacoustic signal:

$$P_n^* = P_1\left[1+\sigma_n e^{\xi}\left(1+(n-1)\sigma_n\xi\right)^{-\frac{n}{n-1}}\right] \qquad (11)$$

From (11) it follows that at $\xi \to 0$,

$$\ln\left(\frac{P_n^*}{P_1}-1\right) \to \ln\sigma_n \ ,$$

i.e.

$$\frac{P_n^*}{P_1}-1=\frac{\delta_n I_0^{n-1}}{\alpha} \qquad (12)$$

Formula (12) allowws us to find the coefficient of multi-photon absorption of δ_n laser beams in liquids on the base of experimental data at simultaneous one-and multi-photon absorptions.

CONCLUSION

The interaction of laser beams with different oil samples is experimentally and theoretically investigated. The character of optoacoustic pressure change in time is confirmed by experiment results. It is established that the opto-acouastic pressure shifts to the region of big *t* with increase of the absorption coefficient. The character of optoacoustic pressure ratio change at linear and non-linear absorption is theoretically established. The formula allowing the confirmation of multiphoton absorption coefficient of laser beams in oil has been obtained. Matlab programming package is used by authors for investigation of physical phenomena and analysis of experimental data.

[1] *Q.Q. Qasanov, A.A. Karabutov, M.A. Musaev, S.F. Osmanov.* Optoakusticheskoe issledovanie maslyanix emulsiy. «Neft I qaz». 1991, №8. (In Russian).

[2] *V.P. Zeleniy, A.A. Karabutov, M.A. Musaev, S.F. Osmanov.* Akusticheskiy jurnal. 1992, t. 38, vip.1, s.53-58. (In Russian).

[3] *M.A. Musaev.* Mexanizm nelineynoqo vzaimodeystviya lazernoqo izlucheniya s veshestvom v infrakrasnoy oblasti spektra. Baku. Izd-vo: Elm. 2004, s.168. (In Russian).

[4] *V.E. Qusev, A.A. Karabutov.* Lazernaya optoakustika. Moskva. «Nauka». 1991, s.304. (In Russian).

Recevied: 29.06.2016

OPTICAL SPECTRA OF HEXAGONAL SELENIUM SINGLE CRYSTALS GROWN FROM THE MELT UNDER HIGH PRESSURE (PART II)

N.Z. JALILOV
Institute of Physics of Azerbaijan NAS
AZ-1143, Baku, H.Javid ave., 33

The reflection spectrum of single crystals of hexagonal selenium grown up from the melt under high pressure in beam energy interval 1-6eV normally incidence on the surface is investigated. The spectral dependences of optical constants and dielectric functions are calculated by Kramers-Kronig method. The optical transitions are confirmed in samples under consideration in photon energy region 1÷6 eV.

Keywords: selenium**,** single crystal, reflection spectrum.
PACS: 535.3; 539.2/6: 539./.04

INTRODUCTION

The electron properties of selenium crystals are studied in series of works [1-17]. The authors [18,19] have synthesized the reflection spectrums of selenium crystals in region 0-30 eV obtained at usual conditions on the base of reflection spectra. They note that the coincidence of experimental and theoretical functions gives the possibility to make the quantum leap in formation of deep and total nature scheme of inherent energy levels and transitions between them under the influence of different external factors (photons, temperature, pressure, electric and magnetic fields and etc).

The obtaining of selenium single crystals at usual conditions is conjugated with big difficulties which are connected with peculiarities of its crystallization. This doesn't allow us to obtain its crystals in big sizes and high purity. However, at high pressures (~4,5 kbar) these disadvantages aren't revealed [23]. The crystal optical spectra grown up under the pressure are studied in the given work.

Note that it is necessary to know the solid substance electron structure, i.e. the dependence of electron energy on wave vector in different energy bands $E_n(k)$ and mutual band positions for revealing of conduction electron movement peculiarity confirming the character of many experimentally observable phenomena. The knowing the electron structures of semiconductors allows us to directly use and change their properties.

It is necessary to note that all empirical calculations of band structure are mainly based on data of optical measurements [24,25]. The experimental data are often used for refinement of theoretical calculation results.

The interaction of the light with substance is described by refraction index and absorption coefficient k which characterize the phase and damping of plane wave in substance. These values can be confirmed from the measurements of substance reflection coefficients which are confirmed on reflected light phase from Kramers-Kroning formula:

$$\theta(E_0) = \frac{E_0}{\pi}\int_0^\infty \frac{\ln R(E)}{E_0^2 - E^2}\, d\omega,$$

$$n = \frac{1-R}{1+R-2\sqrt{R}\cos\theta}, \quad k = \frac{-2\sqrt{R}\sin\theta}{1+R-2\sqrt{R}\sin\theta}.$$

The rest optical parameters are calculated by *n* and *k* values and by formulae alternative from them.

It is necessary to take into consideration the influence of whole spectrum region on reflected light phase for its confirmation from the measurements of reflection coefficient *R(E)*. The extrapolation method *R(E)* on whole unmeasured spectrum region is used by us.

The procedure of semiconductor optical parameter confirmation on the base of experimental data by reflection is expressed in [26]. Moreover, it is necessary that its optical parameters are confirmed in whole region of interband transitions.

It is necessary to note that values of interband transitions for the given material depend on crystallographic directions.

As author mentions [27], only one reflected wave appears at reflection into transparent medium, wave vector is confirmed definitely, independently on surrounding medium properties. At *n* and k are confirmed by complex formulae at beam oblique incidence on the surface. However, these formulae simplify at normal incidence. ε, k and σ parameters at beam reflection in anisotropic mediums have tensor character that is conjugated with significant math difficulties but the general situation keeps the same and the crystal behaves itself as isotropic medium at chosen directions and orientations. However, it is necessary to specially choose the more profitable orientation of crystallographic axis relatively beam surface for more clear revealing of its anisotropy and measurement of corresponding constants.

Thus, the reflection measurement for anisotropic mediums can give whole information on constant values and besides, serve for confirmation of axis orientation in crystal, orientation of reflecting surface, crystal symmetry and etc.

The reflection plays the big role in series of natural phenomena. The perspectives of light reflection application known today for investigation of composition and structure of substance and physical processes taking place in them have the exclusive importance if the information can't be obtain by other way [27].

131 H.Javid ave, AZ-1143, Baku
ANAS, G.M.Abdullayev Institute of Physics
E-mail: jophphysics@gmail.com

The semiconductor optical functions in wide region of fundamental absorption are more effectively studied by the method of almost normal mirror reflection as it is mentioned in [28]. The other clearly optical methods have the essential principle or methodical limits and give the information in limited spectral regions adding the results for almost normal reflection and confirmation at necessity of interband transitions.

As it is mentioned in [29], the less symmetry of anisotropic crystals makes strongly difficult the confirmation of interband ridge displacement in Brillouin band, however, the many ridges form in high symmetry points and they don't reveal the significant dependence on polarization.

The wurtzite hexagonal structure, Brillouin zone of which has 32 symmetry elements and also ZnS (cubic and hexagonal structure) are totally studied from noncubic ones. As author [30] mentions, the zone structure of hexagonal crystals by wurtzite type in points $k=0$ in space along hexagonal axis can be obtained with the help of perturbation theory on corresponding zinc blende. The measurement of their reflection coefficients with non-polarized light shows that their spectra are similar ones and the insignificant shifts in position of first absorption edge from 0,02 up to 0,03 eV are observed at measurements in different directions of linearly polarized light in relation to crystal hexagonal axis.

The reflection spectra at normal light incidence on surface of cubic ZnS and structures by wurtzite type ZnS, CdS, CdSe in nonpolarized light are studied in [31]. Moreover, the distribution directions of incident light either parallel or perpendicular to "c" crystal axis. In first case the results are well coincide with author data for the case of polarized light in $E \| c$ direction and in second one the peaks become less at nonpolarized light.

The investigation of electron structures of anisotropic materials is studied by method of normal incidence at nonpolarized beam in [31-37].

The measurement is carried out at polarized light [33, 35] in several cases for confirmation of ridge displacement in Brillouin zone because of spin-orbit splitting. Usually, the optical parameters in both anisotropic and isotropic materials are confirmed from reflection measurements by method of nonpolarized light normal incident and ridge refinement is carried out with the help of measurement at polarized light in some cases.

The measurement of reflection coefficient $R(E)$ and confirmation of optical parameters of hexagonal selenium single crystals grown up from the melt under high pressure are the aim of the given work.

THE INVESTIGATION TECHNIQUE

The technique of selenium single crystal obtaining under high pressure is described in [23]. The selenium single crystals in ingot form by diameter 1cm and length 4 cm are obtained from the melt under pressure 4,5kbar. At this pressure the crystal growth rate increases in ~10^3 relatively to usual condition because of selenium chain shortening in the melt and decrease of crystallization centers under pressure. The sample crystallographic directions are roentgenographically confirmed.

For sample preparation the material piece is cut off, the surface of which is polished by vibration arrangement or by hand, later it is electrolytically etched in mixture from 5 parts NaOH (10% in water) and one part of tartaric acid (40% in water). After it, the sample surface is treated by etching of impulse current by density ~500 mA/cm^2.

$R(E)$ measurements are carried out in beam energy interval 1÷6 eV normally incident on sample surface. The optical parameters are confirmed by technique of work [26] with the help of special computer programs applied in series of works [38-47].

It is known that according to Maxwell equation all optical parameters are interconnected that is seen from the ratio:

$$\frac{\omega^2}{\upsilon^2} = \frac{\mu}{c^2} 4\pi\sigma(i\omega) + \frac{\mu\varepsilon}{c^2}\omega^2,$$

where ω is cyclic frequency, c is speed of light in vacuum.

THE RESULTS AND THEIR DISCUSSION

$R(E)$ reflection is measured in work and the optical functions are confirmed on its base. Such parameters as: θ reflected light phase; κ absorption and n refraction indexes; real ε_1 and imaginary ε_2 parts of dielectric constant; α absorption coefficient; the function of characteristic volume $-Img\ \varepsilon^{-1}$ and surface $-Img(\varepsilon+1)^{-1}$ electron losses; electro-optical differential functions (α, β); $\varepsilon_2 E$ optical conduction; $\varepsilon_2 E^2$ integral function of bound state density; effective number of valent electrons $N_{ef}(E)$ by $-Img\ \varepsilon^{-1}(E)$ and $-Img(\varepsilon+1)^{-1}(E)$; $\varepsilon_{0,ef}(E)$ effective static dielectric constant, $N_{ef}(E)$ effective number of valent electrons taking part in transitions up to the given energy E are obtained.

R reflection coefficient; electro-optical differential functions (α, β); $\varepsilon_2 E$ optical conduction; $\varepsilon_2 E^2$ integral function of bound state density; effective number of valent electrons $N_{ef}(E)$ by $-\mathrm{Img}\ \varepsilon^{-1}(E)$ and $-Img(\varepsilon+1)^{-1}(E)$; effective static dielectric constant $\varepsilon_{0,ef}(E)$; effective number of valent electrons $N_{ef}(E)$ taking part in transitions up to the given energy E are presented on fig.1-7 from obtained results.

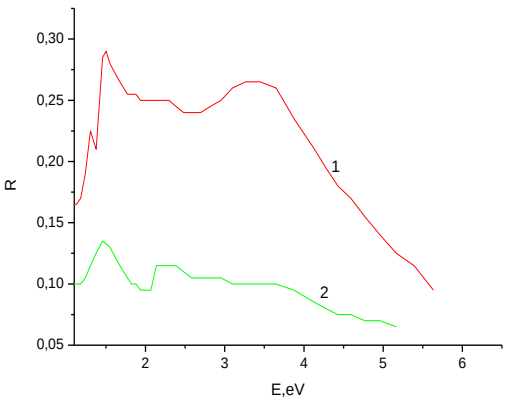

Fig.1. $R(E)$ reflection spectra of hexagonal selenium single crystals which are parallel (curve 1) and perpendicular (curve 2) to "c" axis.

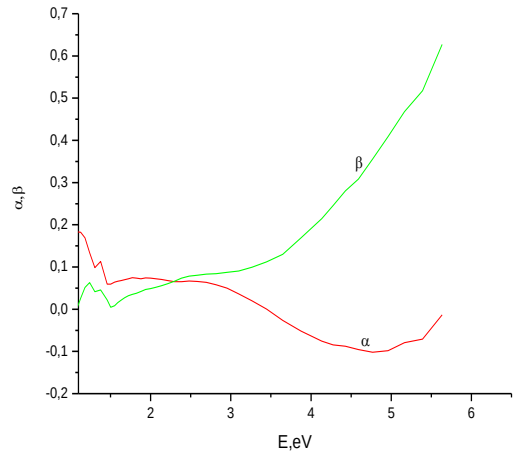

Fig.2. The spectra of electro-optical differential functions (α, β) of hexagonal selenium single crystals parallel to "*c*" axis.

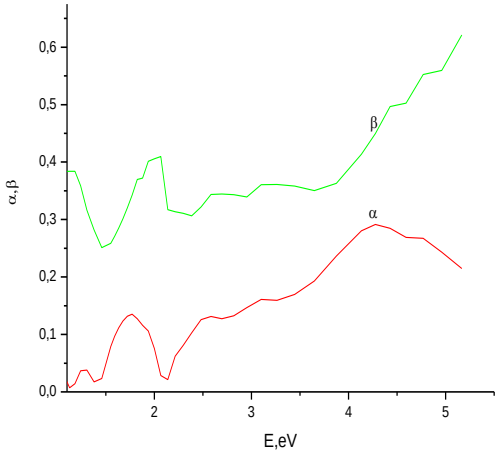

Fig.3. The spectra of electrooptical differential functions perpendicular to "*c*" axis.

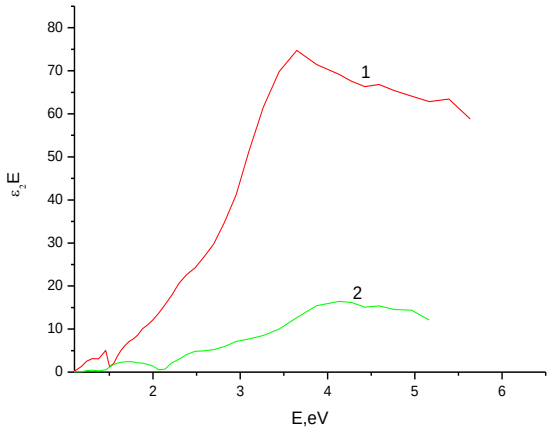

Fig.4. The spectra of $\varepsilon_2 E$ optical conduction of hexagonal selenium single crystals which are parallel (curve 1) and perpendicular (curve 2) to "*c*" axis.

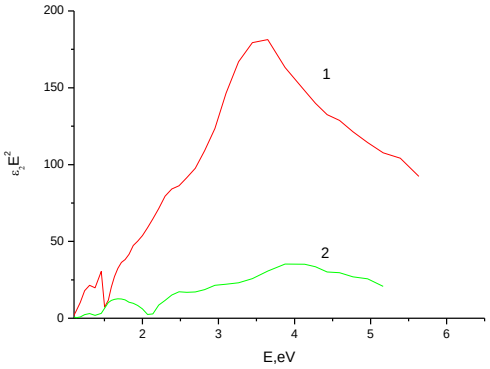

Fig.5. The spectra of $\varepsilon_2 E^2$ integral function of bound state density of hexagonal selenium single crystals which are parallel (curve 1) and perpendicular (curve 2) to "*c*" axis.

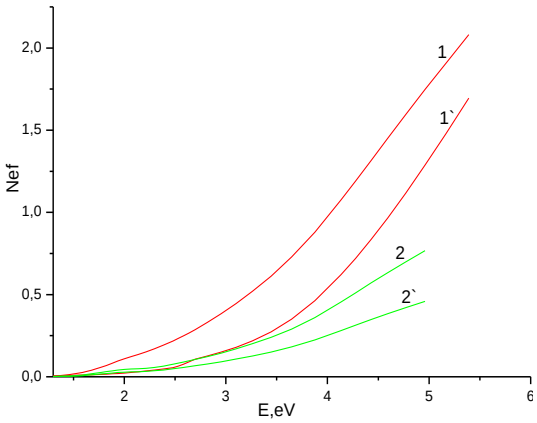

Fig.6. The spectra of effective number of valent electrons $N_{ef}(E)$ $-Im g\varepsilon^{-1}(E)$ and $-Im g(\varepsilon+1)^{-1}(E)$ of hexagonal selenium single crystals which are parallel (curve 1) and perpendicular (curve 2) to "*c*" axis.

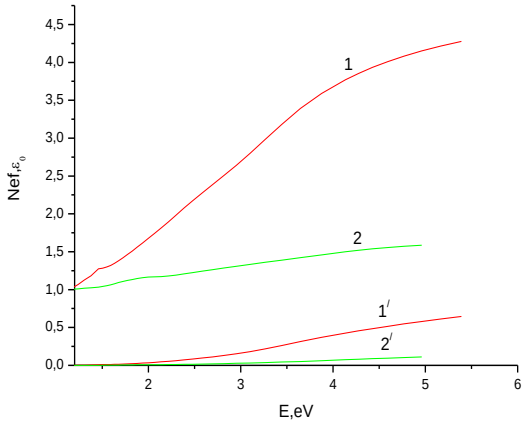

Fig.7. The spectra of $\varepsilon_{0,eff(E)}$ effective static dielectric constant and effective number of valent electrons $N_{ef}(E)$ taking part in transitions up to the given energy E of hexagonal selenium single crystals which are parallel (curve 1,1`) and perpendicular (curve 2,2`) to "*c*" axis.

As it is mentioned in [48], the study of absorption transitions on materials is impossible because of big

absorption value in region of energy interband transitions $E>E_g$ (E_g is minimal energy of interband transitions called forbidden band energy). The reflection stays the unique effective method. On the other hand, the analytical singularities of imaginary parts of complex dielectric constant $\varepsilon_2(E)$ and functions bound by state densities dN/dE almost coincide. The gradient $\nabla_k E_{ij}$ of band-to-band distance makes the main contribution in analytical singularity of dN/dE function.

$$\frac{dN_{ij}}{dE} \sim \int \frac{dS_k}{\left|\nabla_k E_{ij}\right|},$$

where $E_{ij}(k)=E_j(k)-E_i(k)$ is distance between conduction and valence bands. The values dN/dE near critical points in k-space confirmed by $\left|\nabla_k E_{ij}\right|=0$ expression and also the displacement of critical points and transition type. The analysis of $\varepsilon_2(E)$, dN/dE function and $R(E)$ reflection coefficient show that the disposition in energy spectrum and peak character are similar ones or they are very close to these parameters. That's why one can define the values of corresponding interrecord gaps and nature bands with the help of direct coincidence of experimental data on curves and crystal reflection in $E>E_g$ region with theoretical calculations of dN/dE function.

It is known that the least E_g energy between occupied and free states is the one of the very important semiconductor parameters. The high transparency in wide energy region $E<E_g$ is character for non-crystalline materials. The several methods of its definition and evaluations by the level of $\alpha(E)$ absorption coefficient of long-wave absorption edge are known. The exact value of E_g for non-crystalline semiconductors is discussion one and usually, the discussion of $\alpha(E)$ spectrum character in Urbach and Tauz models is carried out without evaluations E_g [49]. E_g is defined by the value of absorption coefficient $\alpha(E) = 10^3 cm^{-1}$ from Tauz model.

As it is mentioned in [49] $N(E)$ density of states is the perception which similarly suitable for both crystalline and non-crystalline substances. By existing results of experimental data the motion of density of states in non-crystalline substance doesn't strongly differ from corresponding one in crystal. The thin structure in first case can be lubricated and the local states can appear in forbidden band, the band structure is kept, i.e. it is defined by atom short-range order in materials.

As it is mentioned in [50] one can't carry out the principal boundary between single monocrystalline, polycrystalline and amorphous substance state. The presence of band structure which is forbidden band and conduction band can be taken from the fact of atom short-range order and for this conclusion there is no need to require the atom periodic disposition. These questions for amorphous and crystalline selenium have been studied in [1,2,51-53], are defined and their electron structures are compared. As it is mentioned in [31] the general scheme of energy bands is mainly defined by crystal structure and material external configuration, but not atoms.

The selenium crystallizes into crystal structure of special type consisting of spiral chains with three atoms in elementary cell. The selenium structure can be also considered as one consisting of three coherent simple hexagonal lattices each of which gives by one atom in elementary cell. The spiral chain radius for selenium is equal 1,07A, the angles between Se-Se-Se atoms in chain are approximately equal to 105^0, the distance between neighbor selenium atoms in the chain is 2.32A, the relation of distances between the neighbor atoms belonging to different chains and one and the same chain is equal to 1,49. That's why it is expected that interaction between atoms in limits of the given chain will be stronger than the one between different chains. Buy this reason, the some selenium main properties can be explained considering the only the separate chain. The analysis of selenium structure symmetry is given by Azendorf [54]. The selenium structure has D_3 group symmetry. The space group isn't symmorphic one and some operations of symmetry are connected with fractional translations. The selenium space group has the screw axes of third order.

The selenium presents itself the elements of sixth group of periodic system, electron configuration of its free electrons (ns^2), n=4.

The internal membranes are totally occupied; the main states with approximately same energies than atoms have correspond them in crystal.

The band structures of selenium and tellurium in one-dimensional approximation are studied by several authors. The early simplest explanation belongs to Reitzu [55], the more detail calculation had been carried out by Olekhno and Nox [56] (in limits of the method of strongly bound electrons with the use of semiemperical screening of exchange potential).

In three-dimensional case the calculation is carried out by Treish and Sandrok [57] (by Green function method).

In selenium the bottom of the conduction band and the top of valent band are in H point taking under the consideration the correspondence between crystalline and atomic wave functions of electrons. It is considered that valent and conduction bands form from p-levels and they can be divided on three regions between which the forbidden energy regions are. It is necessary to note that elements of sixth group of periodic system present all types of electron structures: oxygen and sulphur are isolators, tellurium and tellurium are semiconductors, and polonium is the metal.

Table.

Sample	Optical transitions defined by maximums $\varepsilon_2(E)$ in interval of photon energy 1÷6 eV								
Parallel to «c» axis	1,55	1,65	1,87	2,37	3,43	3,63	-	-	-
Perpendicular to «c» axis	1,54	1,68	1,87	2,38	2,48	2,94	3,87	4,13	4,59

Thus, the spectra of their all optical parameters in energy interval 1-6eV both perpendicular and parallel to "c" axis are defined, the interband optical transitions that gives the possibility to clear their band structures are defined in the given paper on the base of measurement of light reflection in hexagonal selenium single crystals grown up under the pressure 4,5 kbar.

[1] *J.D. Joannopoulos, M. Schlüter and L. Cohen Marvin*. Physical Review B, 11 №6, 1975, 2186-2199.

[2] *A. Vaidyanathan, S.S. Mitra and Y.F.Tsay*, Physical Review B, 21 №6, 1980, 2475-2481.

[3] *L.D. Laude and Fitton, B. Kramer and K. Maschke*. Physical Review Letters, 27 №16, 1971, 1053-1056.

[4] *J.von Boehm and H. Isomäki*. J. Phys. C: Solid St., Phys., 13, 1980, 4953-4963.

[5] *Simpei Tutihasi and Inan Chen*. Physical Review, 158. №3,1967, 623-630.

[6] *W. Henrion*, Phys. Stat. sol. 22, 1967, K33-K37.

[7] *E. Mohler (a), J. Stuke and G. Zimmerer (b).* Phys. Stat. sol. 22, 1967, K49-K52.

[8] *J. Treusch and R. Sandrock*, Phys. Stat. sol. 16, 1966, 487-497.

[9] *B. Kramer and P. Thomas*. Phys. Stat. sol. 26, 1968, 151-157.

[10] *Roly Sandrock*, Physical Review, 169 №3, 1967, 642-650.

[11] *Heikki M. Isomäki*, Physical Review, 26 №8, 1982, 4485-4494.

[12] *V.V. Sobolev*. Dokladi Akademii nauk SSSR, 1963, t. 151, n.6. (in Russian).

[13] *J. Stuke and H. Keller*, Phys. Stat. sol. 7, 1964, 189-203.

[14] *B. Kramer, K. Maschke, L.D. Laude*, Physical Review B, 8 №12, 1973, 5781-5793.

[15] *L.D. Laude, B. Kramer, K. Maschke*, Physical Review B, 8 №12 (1973) 5794-5820.

[16] *Th. Starkloff and J.D. Joannopoulos*, J. Chem. Phys., 68 №2 (1978) 579-584.

[17] *Robert S. Caldwell and H.Y. Fan*, Physical Review, 114 №3, 1959, 664-675.

[18] *V.V. Sobolev.* Elektronnaya struktura khalkogenov. Tez. Dokl. 7-y Vsesoyuz. Konf. Po fizike BUF. Riga: Izd-vo Latv. un-ta, 1986, s. 91. (in Russian).

[19] *V.V. Sobolev.* Elektronnaya struktura khalkogenov. Tez. Dokl. 7-y Vsesoyuz. Konf. «Materialovedenie khalkogenidnikh I kislorodsoderjashikh poluprovodnikov». Chernovtsi: Izd-vo Chernovets un-ta, 1986, 18b. (in Russian).

[20] *S. Tutihasi, Chen* J. Phys. Rev. 158 №3, 1967, 623-630.

[21] *W. Henrion*, Phys. Status Solidi, 22 №1 1967 K33-K37.

[22] *P. Bammes, R. Klucker, E. Koch, T. Tuomi*, Phys. Status solidi (b), 49 №2, 1972, 561-570.

[23] *N.Z. Jaliloz, N.T. Gasanov*. Visokochistie veshestva. №2, 1987, 209. (in Russian).

[24] *I.M. Tsidilkovskiy*. Zonnaya struktura poluprovodnikov. M. Nauka, 1978, 327. (in Russian).

[25] *F. Bassani, J. Pastori Parravichini*. Elektronnie sostoyaniya i opticheskie perekhodi v tverdikh telakh, M., «Nauka», 1982, 391. (in Russian)

[26] Opticheskie svoystva poluprovodnikov *pod red. Bira*, IL, M, 1970, 488. (in Russian).

[27] *V.A. Kizel.* Otrajenie sveta. M., Nauka, 1973, 351. (in Russian).

[28] *V.V. Sobolev, V.V. Nemoshkalenko*. Elektronnaya struktura poluprovodnikov. Kiev nauk. Dumka (1988). (in Russian).

[29] *J. Filips*. Opticheskie spektri tverdikh tel v oblasti sobstvennogo poglosheniya, M. Mir, 1968, 176. (in Russian).

[30] *L. Cohen Marvin and T.K. Bergstresser*, Physical Review, 141 №2 (1966) 789-796.

[31] *D.L. Greenaway and R. Nitsche*, J. Phys. Chem. Solids, 26 1445-1458, 1965.

[32] *D.L. Greenaway and G. Harbeke*, J. Phys. Chem. Solids, 26, 1965, 1585-1604.

[33] *W.S. Walker, J. Osantowski*, Phys. Chem. Solids, 25, 1964, 778-779.

[34] *Joseph L. Birman*, Physical Review, 115 №6, 1959, 1493-1505.

[35] *W.S. Walker*, Physical Review Letters, 13, №2, 1964, 51-52.

[36] *M. Balkanski and Y. Petroff*, Prosseedings of the International Conference on Semiconductors, Paris (1964).

[37] *Manuel Cardona and Gunther Harbeke*, Physical Review, 137 №5A, 1965, A1467.

[38] *N.Z. Jalilov, S.I. Mekhtiyeva, N.M. Abdullayev*. Azerbaijan National Academy of sciences, Series of physical-mathematical and technical sciences physics and astronomy, XXVII №5, 2007, 114. (in Russian).

[39] *N.Z. Jalilov, S.I. Mekhtiyeva, N.M. Abdullayev*. Fizika, XIII №4, 2007, 89. (in Russian).

[40] *N.Z. Jalilov, G.M. Damirov.* Azerbaijan National Academy of sciences, Series of physical-mathematical and technical sciences physics and astronomy, XXVII №5, 2009, 125. (in Russian).

[41] *N.Z. Jalilov, S.I. Mekhtiyeva, N.M. Abdullayev, M.I. Veliyev*. II Ukrainskaya nauch. kon. po poluprovod., 2004, 140. (in Russian).

[42] *N.Z. Jalilov, S.I. Mekhtiyeva, N.M. Abdullayev, M.I. Veliyev*. Azerbaijan National Academy of sciences. Series of physical-mathematical and technical sciences physics and astronomy, XXIV №5(I), 2004. (in Russian).

[43] *S.I. Mekhtiyeva, N.Z. Jalilov, N.M. Abdullayev, N.R. Mamedov*. Dokladi NAN Azerb., LXIII №4, 2007, 48. (in Russian).

[44] *N.Z. Jalilov, N.M. Abdullayev, N.R. Mamedov*. Amorfnie i mikrokristallicheskie poluprovodniki. Sb. trudov VI Mejd. konf., Sankt-Peterburg, 2008, 238. (in Russian).

[45] *N.Z. Jalilov, N.M. Abdullayev, N.R. Mamedov, G.M. Askerov*. Fizika, XIV №3, 2008, 144. (in Russian).

[46] *N.Z. Jalilov, G.M. Damirov*. Trudi X Mejd. konf. «Opto–nanoelektronika, nanotekhnologii i mikrosistemi», Ulyanovsk, 2008, 45. (in Russian).
[47] *N.Z. Jalilov, G.M. Damirov.* Azerbaijan National Academy of sciences. Series of physical-mathematical and technical sciences physics and astronomy, XXVIII №5, 2008, 134. (in Russian).
[48] *J.C. Phillips, Phys. Rev,* 125,1962, 1931, 133, 1964, A452.
[49] *H. Momm, E. Devis.* Elektronnie prochessi v nekristallicheskix veshestvax. Moskva «Mir», 1982. (in Russian).
[50] *A. Rouz.* Osnovi teorii fotoprovodimosti. Izd, Mir, M. 1966. (in Russian).
[51] *N.J. Shevchik, M.Cardona and J.Tejeda*, Physical Review B, 8 №6, 1973, 2833-2841.
[52] *R.H. Williams and J.I.Polanco*, J. Phys C: Solid State Phys., 7, 1974, 2745-2759.
[53] *B. Kramer*, Phys. Stat. sol, 41, 1960, 725-733.
[54] *R.H. Asendorf*, J. Chem. Phys., 27, 1957, 11.
[55] *J.R. Reitz*, Phys. Rev., 105, 1957, 1233.
[56] *D.J. Olechna and R.S. Knox*, Phys. Rev., 140, 1965, A986.
[57] *J. Treusch and R. Sandrock*, Phys. Stat. Solidi, 16, 1966, 487.

Received: 04.07.2016

ADSORBENT REGENERATION BY ELECTRIC DISCHARGE INFLUENCE

A.M. GASHIMOV, K.M. GURBANOV, I.G. ZAKIYEVA, N.M. HOSSEINAHLI
Institute of Physics of Azerbaijan National Academy of Sciences
H.Javid ave., 131, AZ-1143, Baku, Azerbaijan
E-mail: arif@physics.ab.az, magerram-hasanov@rambler.ru

The adsorbent regeneration processes by electric gas discharge influence have been studied. The thermally stimulated relaxation method (TSR) widely used at study of electric charge relaxation in polymer films and other dielectric materials is used for revealing of charged state in natural adsorbents of benthonic clay. The influence of electric fields and discharges on natural adsorbent – bentonite leads to its additional regeneration and simultaneously to appearance of charged state in it.

Keywords: natural adsorbent, regeneration, torch discharge, monomer.
PACS: 52.25-b; 52.80. He; 52.00.00

INTRODUCTION

The main regularities taking place in the system "adsorbent – adsorbate – strong electric field" is necessary to reveal in the connection with big perceptivity of electric control of adsorption processes in problems of purification and liquid separation. The appearance of electric charges of different signs on the surface and in the adsorbent volume is the one of the essential physical factors defining the substance properties [1-4].

It is known that the influence of electric discharge on adsorbents changes their adsorptive capacity [5-7].

The adsorbents are treated by activating influences of different types for increase of efficiency: chemical, radiation, electric and etc. The influences by electric fields and discharges significantly changing the adsorptive capacity of adsorbents are the most effective ones.

The polarization processes in electric field or electric charge introduction directly on the surface or in material volume take place in the result of electric influences on adsorbents in them. The given processes lead to appearance of bound electric charges, i.e. the charged state in material forms [5-8]. As it is mentioned by authors of the given works, the electric charges introduced in adsorbent can be the centers of high adsorption from liquid of different impurities because of the Van-der-Waals force activity in system adsorbent – impurity particle.

The study of different mechanism changes in natural adsorbents treated by electric influences is necessary for solving of task of sorption process intensification with the help of electric discharges.

EXPERIMENT TECHNIQUE AND DISCUSSION OF OBTAINED RESULTS

The investigations of adsorbent regeneration process by influence of electric gas discharge have been carried out in the given paper.

Adsorbent-bentonite is treated by regeneration process in vacuum condition at 180ºC temperature; later the sample is divided into two parts each by 1300mg. Further, 350mg hydrocarbon composition monomer is added in ampoule with bentonite by height 1300mg and 82mg monomer is added in other one and both systems are endured during 24 hours.

The results characterizing the monomer adsorption process are presented in tables 1 and 2.

Table 1.

Monomer, 350 mg	
t, h	m, mg
1	340+1310
2	335+1315
5	330+1320
8	330+1320
24	330+1320

Table 2.

Monomer, 82 mg	
t, h	m, mg
1	72+1310
2	70+1312
5	66+1316
8	66+1316
24	66+1316

From tables 1 and 2 it is seen that adsorbent absorbs the insignificant monomer quantity and total saturation is observed during 5 hours. In further experiments the adsorbents saturated by monomer are treated by regeneration by the way of torch discharge influence in them. The principal electric scheme of material treatment by electric discharge of torch type is presented on fig.1.

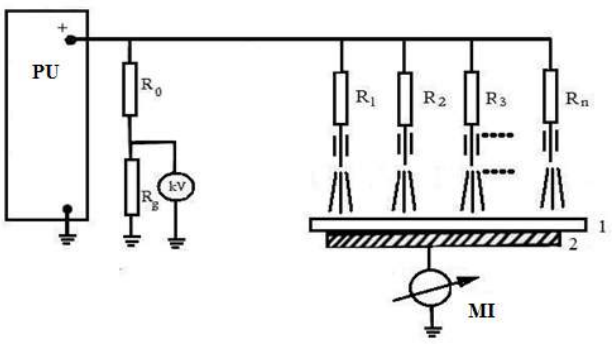

Fig.1. Principal electric scheme:
PU is power unit, kV is kilovolt-meter, R_0, R_g is resistance divisor, $R_1,R\ldots R_n$ are limiting resistors, MI is measuring instrument, 1 is metallic substrate, 2 is electrode.

131 H.Javid ave, AZ-1143, Baku
ANAS, G.M.Abdullayev Institute of Physics
E-mail: jophphysics@gmail.com

Further, the adsorption process is carried out again in previous conditions. The given process results are presented in tables 3 and 4.

The method of thermostimulated relaxation (TSR) widely used at study of electric charge relaxation in polymer films and other dielectric materials is used for revealing of charged state in natural adsorbents of bentonite clay [9].

The experiment of TSR method is carried out by the way of sample heating from room temperature up to 450ºC with constant velocity 2º/min with simultaneous record of relaxation current curve in temperature function (and time) on two-coordinate recorder with amplifier. The heating linearity is supplied by special electron device.

The thermostimulated current curve is shown on fig. 2. The presence of two high-temperature peaks (300ºC, 430ºC) proves the relaxation of electric charges in samples.

The square taken under current curve TSR in time function corresponds to sum charge relaxed in the sample. The charge quantity corresponded to peaks is: Q_1=1,8·10^{-7} coulomb; Q_2=2,8·10^{-7} coulomb.

Table 3.

Monomer, 350 mg	
t, h	m, mg
1	20+1630
2	12+1638
5	8+1642
8	6+1644
24	2+1648

Table 4.

Monomer, 82 mg	
t, h	m, mg
1	18+1364
2	12+1370
5	10+1372
8	8+1374
24	4+1378

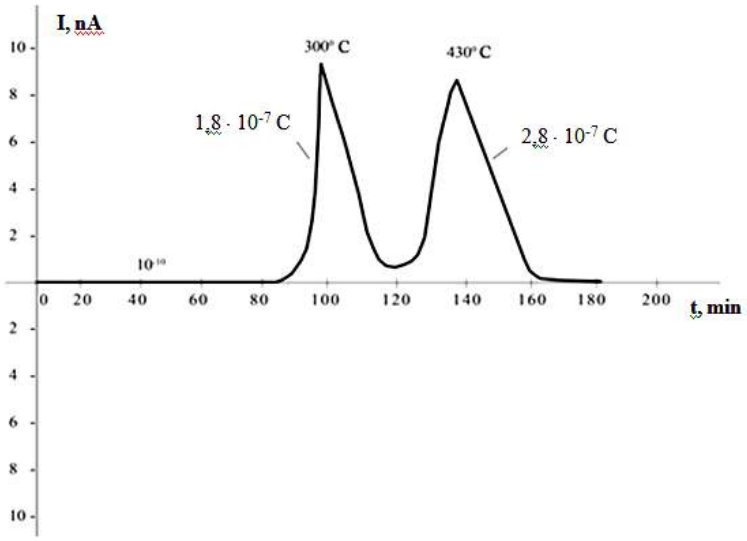

Fig. 2. The curve of thermostimulated current.

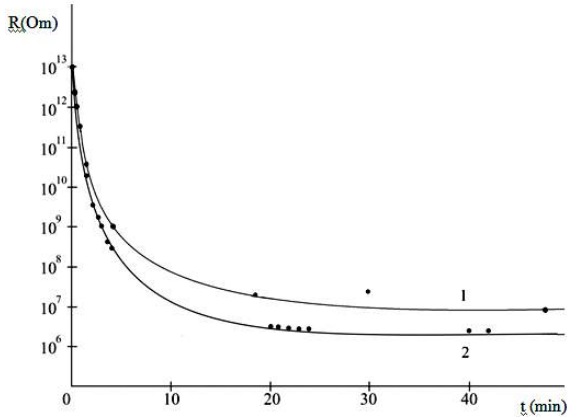

Fig.3. The dependence of bentonite electric resistance on degree of its saturation by steams before and after treatment by torch discharge:
1 is adsorbent nontreated by electric discharge
2 is adsorbent treated by electric discharge

The results of carried investigations show that the adsorption ability of adsorbents increases in many times at their regeneration with torch discharge influence. The fact of increase of bentonite adsorption ability is proved again in further experiments. The bentonite treated by the influence of torch discharge is used in bentonite. The change of adsorbent resistance *fig.3) in dependence on humidification degree before and after treatment is investigated.

The bentonite humidification is carried out by two methods: by the way of water barbotage and also by aging of bentonite portion in atmosphere with humidity 50%. Moreover, the mass change and sample electric resistance are mentioned in definite time periods. The quantity of absorbed water is defined by mass change.

The bentonite intensively adsorbs the steams and in time (approximately after 40 hours) the process transforms into saturation region in initial stages. The measurement of electric resistance through the definite time intervals correspondent to definite humidification degrees allows us to reveal the dependence character of specific resistance change on humidity time (fig.3).

CONCLUSION

Thus, it is shown that the influence of electric fields and discharges on natural adsorbent-bentonite leads to its additional regeneration. This is connected with the fact that the bound water in adsorbent transforms into dissolved state under influence of electric discharge on adsorbent and it easily desorbs. The electro-treatment of adsorbents makes wider the bentonite application in different technological processes.

[1] *M.A. Yegorov.* Voda: ximiya I ekoloqiya. 2008, n.4, s. 41-43. (in Russian).
[2] *Sh. Wang, Y. Peng.* Chemical Engineering Journal. 2010, vol. 156, Issue 1, 11-24.
[3] *A.S. Shilina, V.K. Milinchuk*. Sorbtsionnie i khromatograficheskie protsessi, 2010, t.10, vip. 2, s. 237-245.
[4] *E.S. Klimov, M.V. Buzayeva*. Prirodnie sorbenti i kompleksoni v ochistke stochnikh vod. Ulyanovsk Ul GTU, 2011. 201 s.
[5] *A.M. Gashimov, V.A. Aliyev, K.B. Gurbanov, M.A. Gasanov.* Fizika i khimiya obrabotki materialov, Moskva, 2005, n. 2, s. 86-89.
[6] *M.A. Gasanov.* Fizika i khimiya obrabotki materialov, Moskva, 2006, n. 5, s.88-91.
[7] *A.M. Gashimov, M.A. Gasanov.* Elektronnaya obrabotka materialov. 2008, n. 6, s. 46-51.
[8] *A.M. Gashimov, M.A. Gasanov.* Jurnal Fizicheskoy khimii, 2009, t. 83, n.7, s. 1352-1355.
[9] *G. Sesler.* Elektreti. M.: Mir, 1983, 488 s.

Received: 14.07.2016

131 H.Javid ave, AZ-1143, Baku
ANAS, G.M.Abdullayev Institute of Physics
E-mail: jophphysics@gmail.com

ISSN 1028-8546

2016, Vol. XXII, № 3
Section: En

CONTENTS